Redox Biology 81 (2025) 103580

Contents lists available at ScienceDirect

Redox Biology

journal homepage: www.elsevier.com/locate/redox

Decreased gut microbiome-derived indole-3-propionic acid mediates the exacerbation of myocardial ischemia/reperfusion injury following depression via the brain-gut-heart axis

Xingdou Mu [a,1], Lele Feng [b,1], Qiang Wang [a], Hong Li [a], Haitao Zhou [a], Wei Yi [b,*], Yang Sun [a,**]

[a] Department of Geriatric, XiJing Hospital, Xi'an, Shaanxi, 710000, China
[b] Department of Cardiovascular Surgery, XiJing Hospital, Xi'an, Shaanxi, 710000, China

ARTICLE INFO

Keywords:
Depression
Myocardial ischemia-reperfusion (MI/R)
Gut microbiome
IPA
Ferroptosis

ABSTRACT

Despite the increasing recognition of the interplay between depression and cardiovascular disease (CVD), the precise mechanisms by which depression contributes to the pathogenesis of cardiovascular disease remain inadequately understood. The involvement of gut microbiota and their metabolites to health and disease susceptibility has been gaining increasing attention. In this study, it was found that depression exacerbated cardiac injury, impaired cardiac function (EF%: $P < 0.01$; FS%: $P < 0.05$), hindered long-term survival ($P < 0.01$), and intensified adverse cardiac remodeling (WGA: $P < 0.01$; MASSON: $P < 0.0001$) after myocardial ischemia/reperfusion (MI/R) in mice. Then we found that mice receiving microbiota transplants from chronic social defeat stress (CSDS) mice exhibited worse cardiac function (EF%: $P < 0.01$; FS%: $P < 0.01$) than those receiving microbiota transplants from non-CSDS mice after MI/R injury. Moreover, impaired tryptophan metabolism due to alterations in gut microbiota composition and structure was observed in the CSDS mice. Mechanistically, we analyzed the metabolomics of fecal and serum samples from CSDS mice and identified indole-3-propionic acid (IPA) as a protective agent for cardiomyocytes against ferroptosis after MI/R via NRF2/System xc-/GPX4 axis, played a role in mediating the detrimental influence of depression on MI/R. Our findings provide new insights into the role of the gut microbiota and IPA in depression and CVD, forming the basis of intervention strategies aimed at mitigating the deterioration of cardiac function following MI/R in patients experiencing depression.

1. Introduction

Cardiovascular disease (CVD) and depression are currently the two most common causes of disability in high-income countries and are projected to reach this status across countries of all income levels by 2030 [1]. Comorbid CVD and depression are associated with increased mortality, excess disability, greater healthcare expenditure, and reduced quality of life [2]. Patients with CVD experience more depression than the general population. Meanwhile, patients with depression exhibit a higher propensity for developing CVD compared to the general population [3,4]. Furthermore, the presence of depressive symptoms has been independently associated with increased rates of cardiac and all-cause mortality, higher rehospitalization incidence, and reduced quality of life following acute myocardial infarction [5,6]. Additionally, the European Society of Cardiology recognizes depression as an independent cardiovascular risk factor in individuals with heart disease [7]. Therefore, elucidating the underlying systemic and molecular mechanisms connecting these two conditions is crucial for improving human health.

The gut microbiota, also termed the "second brain," exhibits bidirectional communication with the central nervous system through the "microbiota-gut-brain" axis under physiological and pathological conditions [8–11]. Depression is usually associated with microbial dysbiosis, resulting in alterations in microbial diversity owing to the disrupted equilibrium of the microbiota and the accompanying functional changes [12]. An increasing number of preclinical and clinical studies have highlighted the association between compositional and functional (e.g., metabolite) changes in the gut microbiota and the onset and progression

* Corresponding author.
** Corresponding author.
E-mail addresses: yiwei@fmmu.edu.cn (W. Yi), drsunyang@fmmu.edu.cn (Y. Sun).
[1] Contributed equally.

https://doi.org/10.1016/j.redox.2025.103580
Received 6 February 2025; Received in revised form 11 February 2025; Accepted 19 February 2025
Available online 5 March 2025

of depression via regulation of the gut-brain axis [12–14]. Simultaneously, gut microbiota can directly influence the onset and progression of coronary heart disease through their metabolites, including bile acids, steroids, short-chain fatty acids, and trimethylamine N-oxide [15–17]. Consequently, gut microbiota and their metabolites may serve as critical links between depression and cardiovascular diseases.

Gut microbiota directly metabolize tryptophan within the gastrointestinal tract, producing bioactive compounds such as serotonin, kynurenic acid, and indole-3-propionic acid (IPA), which subsequently influence various physiological processes [18,19]. Among these

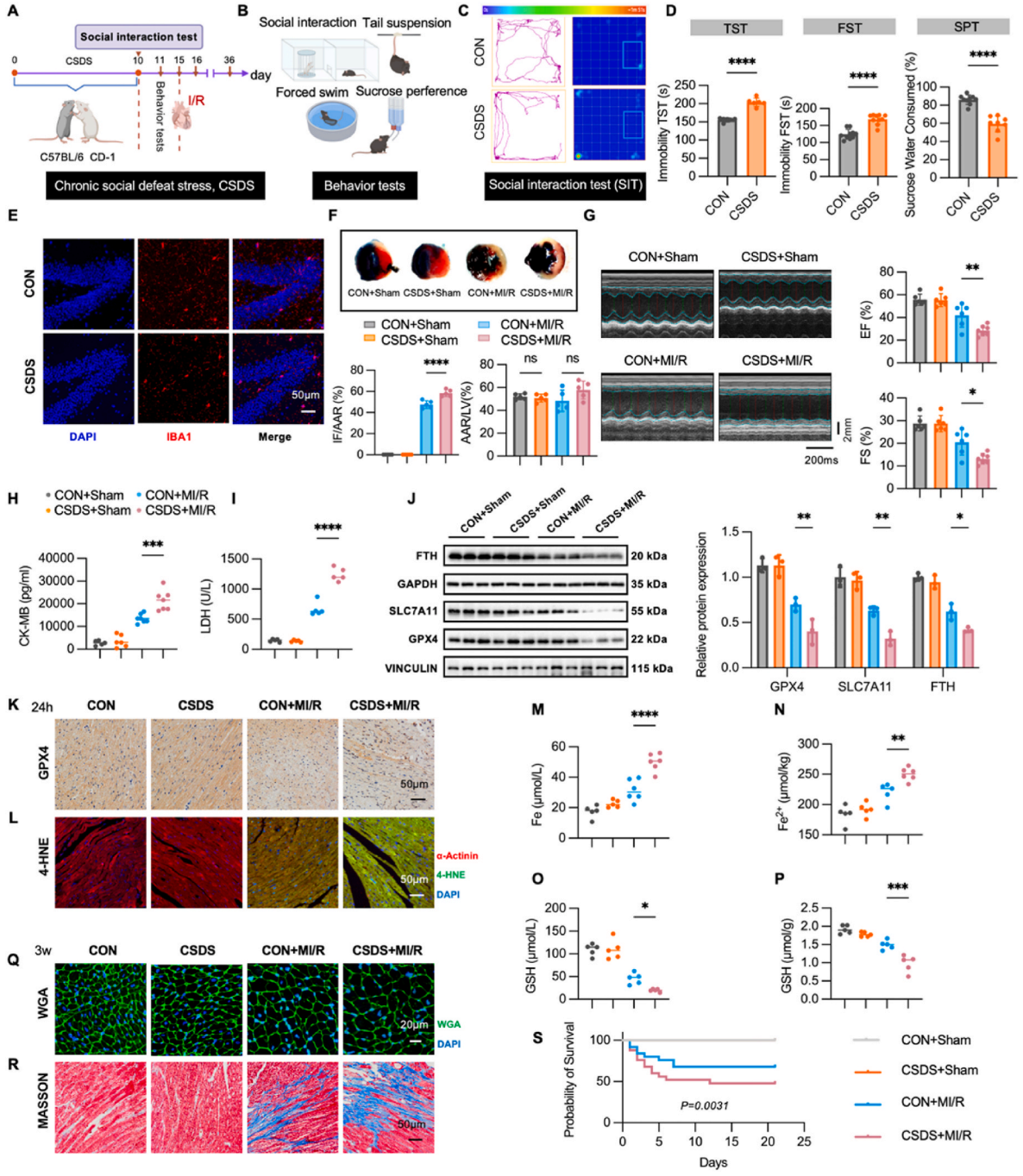

Fig. 1. Chronic social defeat stress (CSDS) induces significant depression- and anxiety-like behaviors, aggravates cardiac dysfunction, hinders long-term survival, and intensifies adverse cardiac remodeling post-myocardial ischemia/reperfusion (MI/R). (A) Experimental design. (B) Behavior tests. (C) Representative activity tracking during the social interaction test (SIT) for control and CSDS mice in the presence of a CD1 target (Plot shows a heat map of the animal's center point, for the entire duration of the test, and uses the scale shown below). (D) Tail suspension test (TST), forced swimming test (FST), and sucrose water preference test (SPT) of the control and CSDS groups. (E) The immunofluorescent staining of IBA1 in the DG region of the hippocampus in control and CSDS mice. (F) Triphenyltetrazolium chloride (TTC) staining of heart tissue. (G) Transthoracic echocardiography of mice. EF%, ejection fraction; FS%, fractional shortening. (H) The creatine kinase MB (CK-MB) levels in serum. (I) The lactate dehydrogenase (LDH) levels in serum. (J) Relative proteins expression of ferroptosis in heart tissue. (K) The immunohistochemistry staining of glutathione peroxidase 4 (GPX4) in the heart tissue. (L) The immunofluorescent staining of 4-hydroxy-2-nonenal (4-HNE) in heart tissues. (M − N) Total and ferrous iron levels in serum and heart tissue. (O–P) Glutathione (GSH) levels in serum and heart tissue. (Q) Wheat germ agglutinin (WGA) staining of heart tissues. (R) Masson staining of heart tissues. (S) The 3-week survival of mice. Data are expressed as mean ± standard error (SE), n = 3–10, ns, no significance, $^{*}p < 0.05$, $^{**}p < 0.01$, $^{***}p < 0.001$, $^{****}p < 0.0001$.

metabolites, IPA exhibits cardioprotective and nerve repair effects in animal models [20–22]. Alterations in plasma IPA levels have been reported in patients with major depressive disorder (MDD) [23]. However, the potential role of the IPA in the association between depression and cardiovascular disease remains unclear. In this study, we investigated the potential role of gut microbiota and their metabolites in mice with exacerbated cardiovascular disease in the context of depression.

2. Results

2.1. Chronic social defeat stress (CSDS) induces significant depression- and anxiety-like behaviors, aggravates cardiac dysfunction, hinders long-term survival, and intensifies adverse cardiac remodeling post-MI/R

CSDS paradigm was used to induce depression and anxiety in mice (Fig. 1A). After that, different behavioral tests were performed (Fig. 1B). Stressed mice exhibited social avoidance behaviors after 10 days of CSDS, indicating that the test mouse predominantly avoided the social interaction in the presence of a CD-1 partner mouse, as evidenced by behavioral heatmaps from both CON and CSDS mice (Fig. 1C). Stressed mice also showed depression-like phenotypes, such as behavioral despair, as indicated by spending less time struggling in the tail suspension test (TST) and forced swimming test (FST), and the consumption of significantly less sucrose water in the sucrose water preference test (SPT) (Fig. 1D). The hippocampus plays a critical role in emotional and cognitive processing [24,25], and increased infiltration of microglia into the hippocampus has been implicated in the onset and progression of anxiety and depression [26]. We observed an increase in the number of microglial cells in the dentate gyrus (DG) region of the hippocampus in CSDS mice (Fig. 1E). We evaluated the myocardial infarct size and cardiac function and found that stressed mice were afflicted by more severe myocardial damage post-MI/R, represented by a larger myocardial infarct size and decreased EF% and FS% compared to those of non-CSDS mice (Fig. 1F and G). The CSDS mice also showed enhanced creatine kinase MB (CK-MB) and lactate dehydrogenase (LDH) levels (Fig. 1H and I) after MI/R. Ferroptosis is recognized as a critical factor in MI/R injury, primarily attributed to impairment of the cellular antioxidant system, notably the system xc−-glutathione (GSH)-glutathione peroxidase 4 (GPX4)-dependent antioxidant defense mechanism [27–29]. Western blot analysis showed that CSDS downregulated the expression of GPX4, ferritin heavy chain (FTH), and solute carrier family 7 member 11 (SLC7A11) in the heart tissue of mice after MI/R injury (Fig. 1J). Furthermore, we observed IL-1β, IL-6, acyl-CoA synthetase long-chain family member 4 (ACSL4), and prostaglandin-endoperoxide synthase 2 (PTGS-2) mRNA expressions increased, whereas that of GPX4 decreased in the heart tissue of CSDS mice after MI/R injury (Figs. S1A–S1E). Meanwhile, immunohistochemical (IHC) staining showed that the expression of GPX4 decreased in both the CSDS and non-CSDS groups after MI/R. And this reduction was more pronounced in the CSDS group (Fig. 1K). 4-hydroxy-2-nonenal (4-HNE) is a recognized by-product of lipid peroxidation and serves as a biomarker for ferroptosis [30,31]. And the accumulation of 4-HNE has been observed in a range of cardiovascular pathologies, including MI/R injury [32,33]. Immunofluorescence (IF) staining showed that the expression of 4-HNE and reactive oxygen species (ROS) level increased more significantly in the CSDS group compared with non-CSDS group after MI/R (Fig. 1L and S1J). In addition, as an indispensable element of ferroptosis, a more significant increase in total and ferrous iron levels was observed in the CSDS group after MI/R (Fig. 1M and N). At the same time, GSH was significantly decreased in the serum and heart of CSDS mice after MI/R injury compared to those of non-CSDS mice, as shown in Fig. 1O and P. Three weeks after MI/R, wheat germ agglutinin (WGA) staining revealed a more prominent enlargement in the cardiomyocyte cross-sectional area in the CSDS group (Fig. 1Q). Meanwhile, Masson's staining revealed a significantly greater increase in post-MI/R cardiac fibrosis in the border region of CSDS mice following MI/R. (Fig. 1R). Notably, a significant reduction in post-MI/R survival was observed in the CSDS group compared to the control mice (Fig. 1S). Collectively, these data consistently demonstrate that CSDS can aggravate cardiac dysfunction post-MI/R in mice, hinders long-term survival, and intensifies adverse remodeling following MI/R.

2.2. Fecal microbial transplantation (FMT) from depressed mice aggravates cardiac dysfunction and cardiac remodeling, hinders long-term survival post-MI/R

The gut microbiota has been reported to be associated with many diseases, such as depression and anxiety [12,34]. Here, we sought to determine whether the susceptibility of CSDS mice to MI/R is transmissible by fecal microbial transplantation using fecal samples from CSDS mice. Male C57BL/6 mice were administered oral antibiotic cocktail (ABX) for 10 days to deplete the original gut microbiota and facilitate the colonization of the gut microbiota. After that, daily gavage of gut microbiota from CON or CSDS mice was performed for 2 weeks (Fig. 2A). We observed that mice receiving microbiota transplants from CSDS mice (ABX + FMT (CSDS) + MI/R) had worse cardiac function and larger myocardial infarct size after MI/R than those receiving microbiota transplants from CON mice (ABX + FMT (CON) + MI/R) (Fig. 2B and C). Additionally, higher CK-MB and LDH levels were observed in the ABX + FMT (CSDS) + MI/R group (Fig. 2D and E). The expression levels of GPX4, FTH, and SLC7A11 were lower in the ABX + FMT (CSDS) + MI/R group than in the ABX + FMT (CON) + MI/R group (Fig. 2F). As shown in Fig. 2G and H, and Fig. S2G, we further verified that GPX4 levels decreased, 4-HNE and ROS levels increased in mice that received the CSDS gut microbiota after MI/R. In addition, total iron and ferrous ions were elevated in the ABX + FMT (CSDS) + MI/R group (Fig. 2I and J). Moreover, GSH levels were significantly decreased in the serum and heart of the ABX + FMT (CSDS) + MI/R group compared with those in the ABX + FMT (CON) + MI/R group, as shown in Fig. 2K and L. Mice receiving CSDS gut microbiota transplantation showed significantly elevated levels of heart IL-1β, IL-6, and TNF-α mRNA expressions compared to the ABX + FMT (CON) + MI/R group (Figs. S2A–S2C). The lipid peroxidation index levels of ACSL4 and PTGS-2 increased, whereas that of GPX4 significantly decreased in the ABX + FMT (CSDS) + MI/R group (Figs. S2D–S2F). Three weeks post-MI/R, as illustrated in Fig. 2M and N, fecal transplantation from the CSDS mice exacerbated cardiac remodeling in MI/R mice. This exacerbation was evidenced by increased cardiac fibrosis and the enlargement of cross-sectional cardiomyocyte areas. Of note, a significant reduction in post-MI/R survival was also observed in the ABX + FMT (CSDS) + MI/R group compared to the ABX + FMT (CON) + MI/R (Fig. 2O). Thus, these findings corroborate the involvement of gut microbiota in exacerbating cardiac dysfunction and remodeling in CSDS mice following MI/R. Additionally, the transplantation of gut microbiota from the CSDS mice could impede long-term survival post-MI/R.

2.3. Depression changes gut microbial richness and community structure

To identify whether CSDS modulates gut microbial content and composition, metagenomics of fecal samples from CON and CSDS mice was performed to analyze the bacterial taxonomic composition. Fifteen samples obtained from the two groups (CON, n = 7; CSDS, n = 8) were sequenced to generate gene profiles. Overall, 70.64 (GB), and 81.038 (GB) raw bases were obtained for the CON and CSDS groups, respectively. Alpha diversity reflects the richness and diversity of microbiota. No significant differences were observed in the Simpson and Shannon indices between the two groups (Fig. 3A and B). We used Bray–Curtis Principal coordinate analysis (PCoA), Principal component analysis (PCA), and Nonmetric multidimensional scaling (NMDS) to examine the community structures of the gut microbiota and found that the gut microbiota of mice in the CSDS group was distinct from that of the CON group (Fig. 3C–E). In the fecal samples of these mice, the phylum

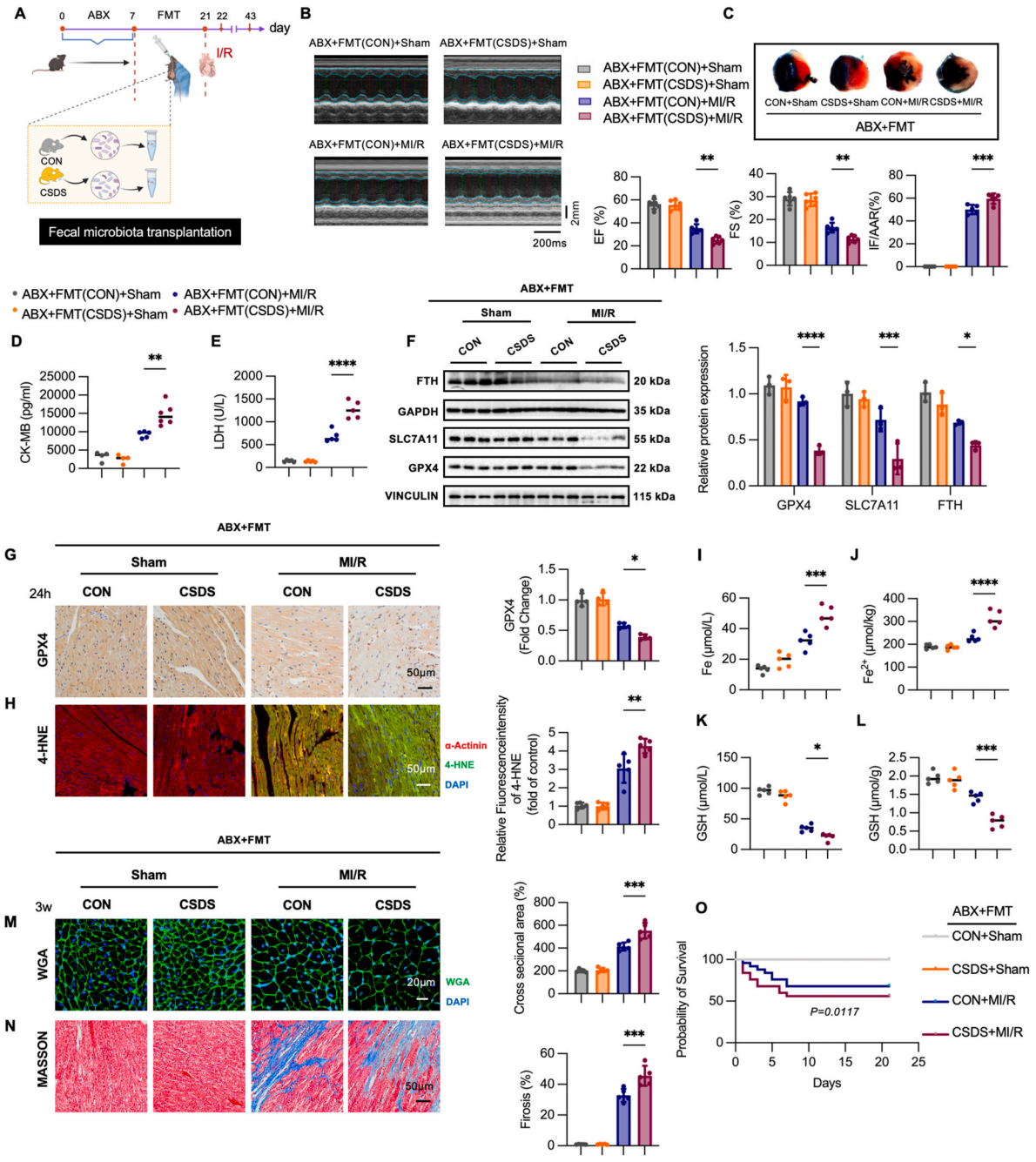

Fig. 2. Fecal microbial transplantation from CSDS mice aggravates cardiac dysfunction, hinders long-term survival, and intensifies adverse cardiac remodeling post-MI/R. (A) Experimental design. (B) Transthoracic echocardiography of mice. (C) TTC staining of heart tissue. (D) The CK-MB levels in serum. (E) The LDH levels in serum. (F) Relative expression of ferroptosis-related proteins in heart tissue. (G) The immunohistochemistry staining of GPX4 protein in heart tissue. (H) The immunofluorescent staining of 4-HNE in heart tissues. (I–J) Total and ferrous iron levels in serum and heart tissue. (K–L) GSH levels in serum and heart tissue. (M) WGA staining of heart tissues. (N) Masson staining of heart tissues. (O) The 3-week survival of mice. Data are expressed as mean ± SE, n = 3–6, ns, no significance, $^{*}p < 0.05$, $^{**}p < 0.01$, $^{***}p < 0.001$, $^{****}p < 0.0001$.

Bacteroidetes was predominant, accounting for 56.8 %–80.2 % of the gene sequences. The second most abundant phylum was Firmicutes, comprising 9.8 %–38.6 % of the sequences in each group (Fig. 3F). At the species level, *s_Candidatus_Amulumruptor _caecigallinarius*, *s_ Chlamydia_abortus*, and *s_ Bacteroides_aciditaciens* were the predominant microflora (Fig. 3G). Firmicutes and Bacteroidetes are the dominant phyla, and the *Firmicutes/Bacteroidetes* ratio is considered an indicator of intestinal disorders [35]. Interestingly, as shown in Fig. 3H and I, Firmicutes was higher abundant and Bacteroidetes was lower abundant than in the non-CSDS group. The *Firmicutes/Bacteroidetes* ratio is also increased in the CSDS group compared to the CON group (Fig. 3J). Cladograms representing the relationships between biomarker taxa were generated using LEfSe analysis (Fig. 3K). We identified different distributions of 20 bacteria (e.g., *Bacteroides, Akkermansia, Lactobacillus, Prevotella, and Alistipes)* between the two groups (Fig. 3L). Untargeted metabolomic analysis of fecal samples was performed to examine the interaction between gut microbiota and host metabolism. As shown in Fig. 3M, enriched metabolic pathways were derived by calculating the ratio of the number of differential metabolites annotated in each pathway to the total number of differential metabolites. Amino and nucleotide sugar metabolism (31.2 %), tryptophan metabolism (28.21 %), purine metabolism (25.21 %), and steroid hormone biosynthesis

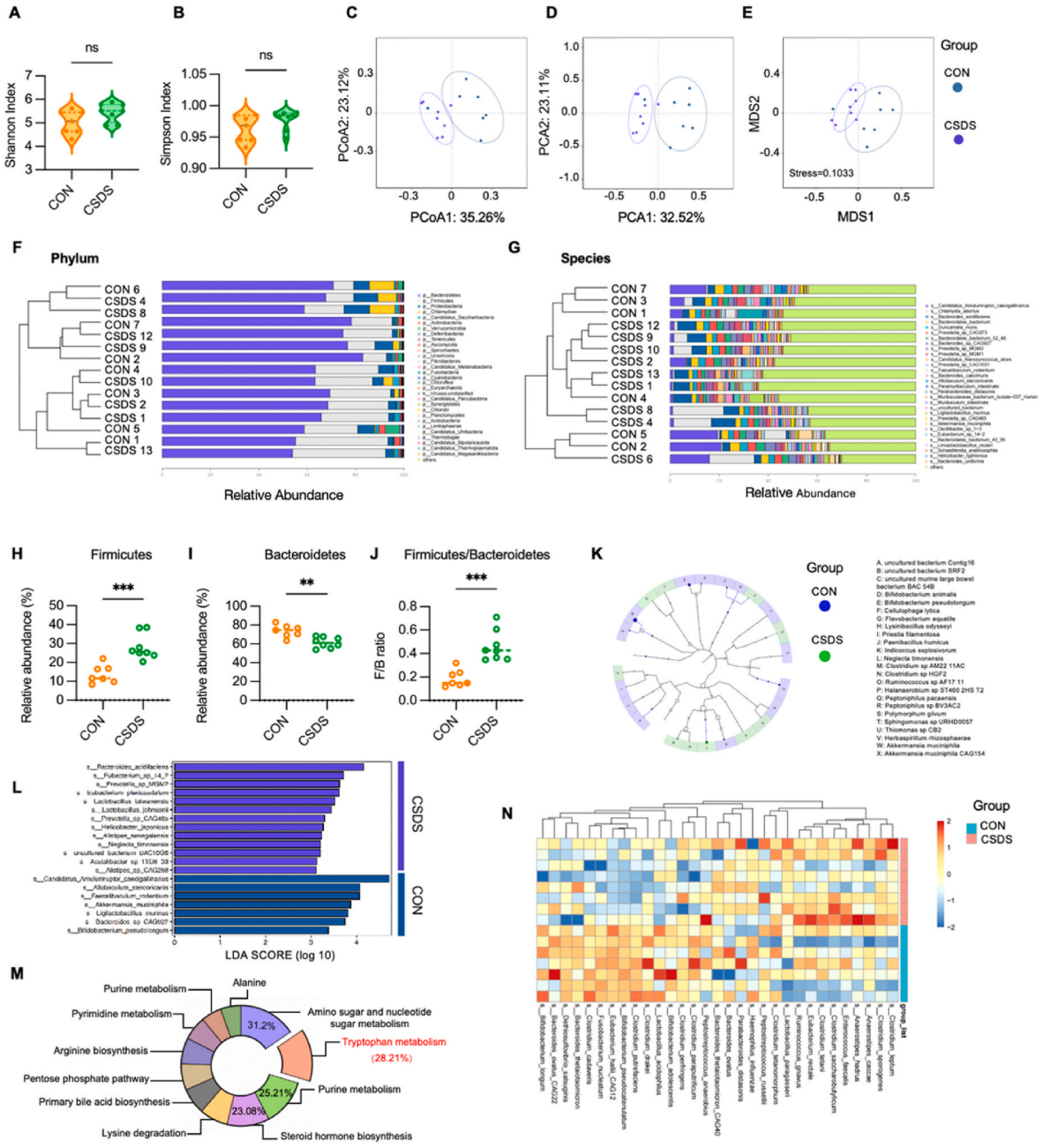

Fig. 3. CSDS changes gut microbial richness and community structure. (A–B) Alpha diversity evaluation of colon microbial richness and evenness by measuring Simpson and Shannon diversity indexes. (C–E) Principal coordinate analysis (PCoA) score plot; Principal component analysis (PCA); Nonmetric multidimensional scaling (NMDS) score plot based on the operational taxonomic unit (OUT) of the gut microbe. (F) Unweighted pair-group method with arithmetic mean (UPGMA) analysis (at the phylum level). (G) UPGMA analysis (at the species level) in the mice cecum of the control and CSDS groups. (H–I) The relative abundance of Firmicutes and Bacteroidetes. (J) The ratio of Firmicutes/Bacteroidetes. (K) Linear discriminant analysis effect size (LEfSe) was performed to identify the bacteria that are differentially represented between the different groups. (L) The Linear Discriminant Analysis (LDA) score. (M) The untargeted metabolomic analysis of fecal samples. (N) Relative abundance of tryptophan related gut microbiota. Data are expressed as mean ± SE, n = 7–8, ns, no significance, $*p < 0.05$, $**p < 0.01$, $***p < 0.001$.

(23.08 %) were the dominant enriched metabolic pathways. Among them, tryptophan, which is an essential amino acid acquired through dietary intake, is integral to protein biosynthesis and serves as a precursor for the synthesis of numerous bioactive compounds, thereby influencing various pathophysiological processes including depression and CVD [21,36–39]. Furthermore, we conducted an analysis of the gut microbiota involved in tryptophan metabolism, including *Peptostreptococcus* spp., *Lactobacilli., Lactobacillus* spp., *Bifidobacterium* spp., *etc.* [19]. As shown in Fig. 3N, the relative abundances of *Bifidobacterium, Lactobacillus* and *Parabacteroides* were significantly higher in the CON group than in the CSDS group, whereas no significant difference was observed in the relative abundances of *Peptostreptococcus* and *Limosilactobacillus* between the two groups. These results indicate that the composites and structure of the gut microbiota, especially those related to tryptophan metabolism, were significantly altered in the context of depression.

2.4. Tryptophan supplementation alleviates cardiac dysfunction and cardiac remodeling post-MI/R in CON but not in CSDS mice

A tryptophan supplementation model was used to elucidate whether the altered tryptophan metabolism is responsible for the increased susceptibility of CSDS mice to MI/R (Fig. 4A). Interestingly, we observed that although tryptophan supplementation significantly improved cardiac function in the CON + Trp + MI/R group, no improvements were observed in EF% and FS% in the CSDS + Trp + MI/R group (Fig. 4B). Similarly, the myocardial infarct size in CSDS mice was not improved by tryptophan supplementation compared to that in CON mice (Fig. 4C). We found that supplementation with tryptophan significantly reduced CK-MB and LDH levels in the CON + Trp + MI/R group, while no improvements in CK-MB and LDH levels were observed in the CSDS + Trp + MI/R group (Fig. 4D and E). The protein expression of GPX4, SLC7A11, and FTH in the CSDS + Trp + MI/R group were downregulated compared to those in the CON + Trp + MI/R group, as shown in Fig. 4F. Decreased mRNA expression levels of IL-1β, IL-6, PTGS-2, and ACSL4, and increased expression levels of GPX4 (Figs. S4A–S4C) were found in the CON + Trp + MI/R group but not in the CSDS + Trp + MI/R group. While tryptophan supplementation decreased the Fe and Fe^{2+} levels in the CON + Trp + MI/R group, we did not observe a significant

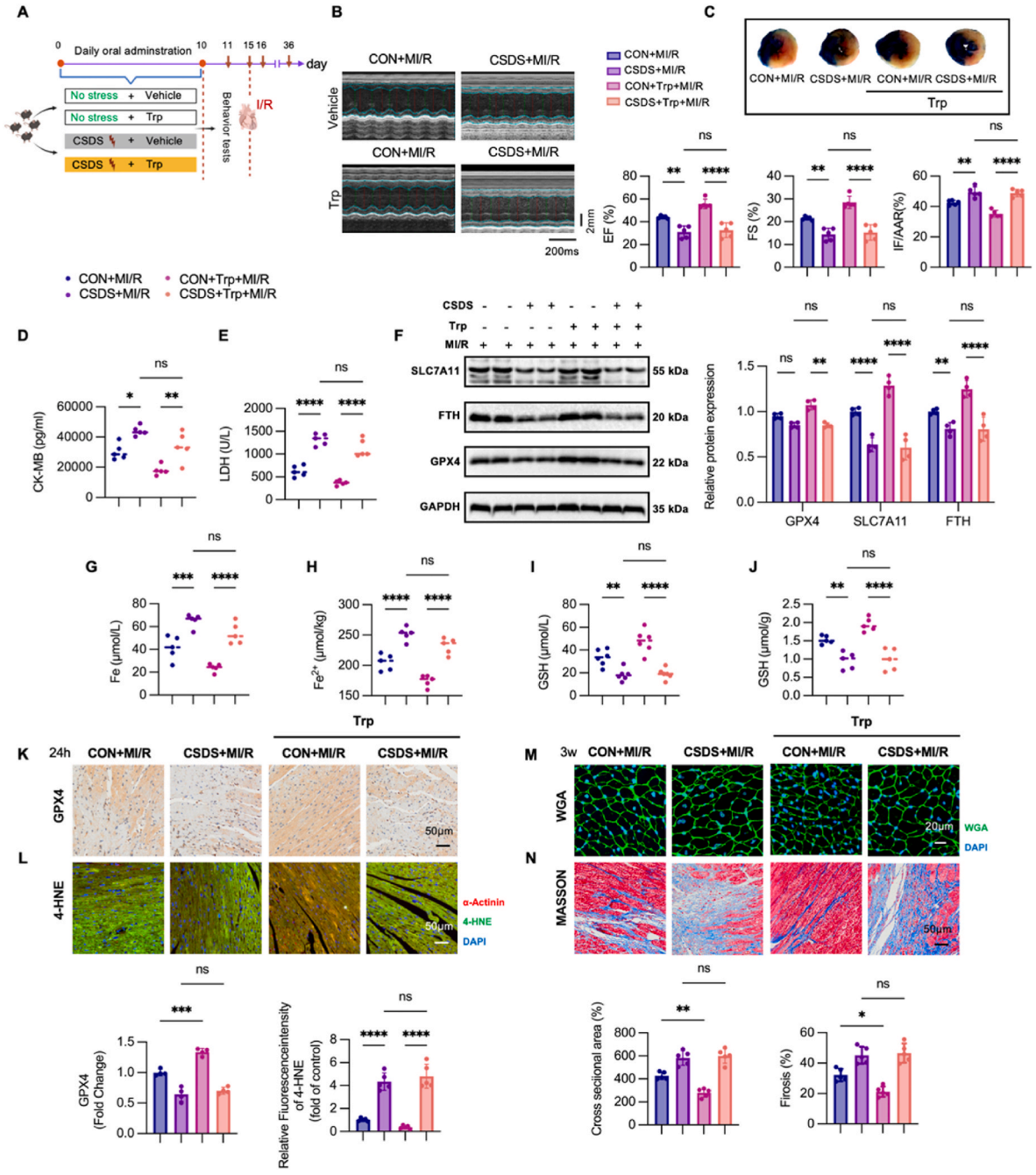

Fig. 4. Tryptophan supplementation alleviates cardiac dysfunction and cardiac remodeling post-MI/R in CON but not in CSDS mice. (A) Experimental design. (B) Transthoracic echocardiography of mice. (C) TTC staining of heart tissue. (D) The CK-MB levels in serum. (E) The LDH levels in serum. (F) Relative proteins expression of ferroptosis in heart tissue. (G–H) Total and ferrous iron levels in serum and heart tissue. (I–J) GSH levels in serum and heart tissue. (K) The immunohistochemistry staining of GPX4 protein in heart tissue. (L) The immunofluorescent staining of 4-HNE protein in heart tissue. (M) WGA staining of heart tissues. (N) Masson staining of heart tissues. Data are expressed as mean ± SE, n = 3–6, ns, no significance, *$p < 0.05$, **$p < 0.01$, ***$p < 0.001$, ****$p < 0.0001$.

reduction in the Fe and Fe^{2+} levels in the CSDS + Trp + MI/R group (Fig. 4G and H). Moreover, GSH levels in the serum and heart were increased in the CON + Trp + MI/R group. Whereas, no significant difference was observed between the CSDS + Trp + MI/R and CSDS + MI/R groups (Fig. 4I and J). Furthermore, immunohistochemical analysis revealed that, notwithstanding tryptophan supplementation, the expression levels of GPX4 did not exhibit an increase in the CSDS + Trp + MI/R group following MI/R (Fig. 4K). IF staining also showed that the expression of 4-HNE and ROS level were higher in the CSDS + Trp + MI/R group than in the CON + Trp + MI/R group (Fig. 4L and S4F). The staining of heart sections 3 weeks following MI/R indicated that tryptophan supplementation significantly ameliorated myocardial fibrosis and cardiac remodeling in the CON + MI/R group. However, it did not exhibit a statistically significant effect on the CSDS + MI/R group (Fig. 4M and N). Collectively, these findings suggest that CSDS altered the composition and richness of the gut microbiota of tryptophan metabolism, thereby modifying the ability to metabolize tryptophan. Ultimately, these alterations nullified the cardioprotective effect of tryptophan.

2.5. Reduced IPA level in mice with CSDS

Given the crucial role of altered tryptophan metabolism in CSDS mice, we performed tryptophan-targeted metabolomics of the serum from CON and CSDS mice to determine the metabolic signatures of tryptophan metabolism in depression. PCA plots revealed distinct clusters in samples from the CON and SDS mice (Fig. 5A). The metabolites in the tryptophan metabolism pathway were significantly different in serum from CSDS mice compared to those from CON mice (Fig. 5B). L-tryptophan, kynurenic acid, NAD, xanthurenic acid, indole acrylic acid (IA), and indole-3-aldehyde (IAld) levels were decreased in CSDS mice (Fig. 5C). Additionally, we screened metabolites exhibiting a VIP score greater than 1 or those demonstrating a fold change of either $\geq$2 or $\leq$0.5. Notably, CSDS mice showed decreased levels of a series of metabolites, such as IPA and indole acetic acid (IAA) (Fig. 5D).

2.6. IPA supplementation rescued cardiac dysfunction and cardiac remodeling post-MI/R in CSDS mice resulted by impaired tryptophan metabolism

Eight-week-old male C57BL/6 mice were treated with IPA (20 mg/kg BW) or tryptophan (2 g/kg BW) daily by oral gavage for 10 days to directly test whether dietary IPA supplementation affects the development of MI/R (Fig. 6A). Despite the fact that tryptophan supplementation missed in improving cardiac function in CSDS mice after MI/R, we observed that mice treated with IPA showed significantly elevated EF% and FS% after MI/R (Fig. 6B). IPA supplementation also decreased the myocardial infarct size in CSDS mice after MI/R, as shown in Fig. 6C. Meanwhile, IPA supplementation resulted in reduced CK-MB and LDH levels of CSDS mice after MI/R (Fig. 6D and E). The inflammatory cytokines IL-1β and IL-6 also decreased in the CSDS + MI/R group after IPA supplementation (Figs. S5A and S5B). We then assessed the mRNA expression of key players associated with ferroptosis. Among them, GPX4 increased, whereas ACSL4 and PTGS-2 decreased after IPA supplementation in the CSDS + MI/R group (Figs. S5C–S5E). Similar results were confirmed by western blotting analysis of ferroptosis-related proteins. IPA supplementation significantly increased the proteins expression of GPX4, FTH, and SLC7A11 in the CSDS + MI/R group compared to tryptophan supplementation (Fig. 6F). Given that nuclear factor erythroid 2-related factor 2 (NRF2) has been documented to counteract MI/R injury and ferroptosis [40,41], we quantified the expression levels of NRF2 in mice cardiac tissue. Consistent with our hypothesis, supplementation with IPA resulted in an upregulation of NRF2 expression in CSDS mice after MI/R. The iron content in the serum and heart decreased in IPA supplementation mice (Fig. 6G and H) and it also increased GSH concentrations in the serum and heart both in the CON + IPA + MI/R group and CSDS + IPA + MI/R group (Fig. 6I and J). Moreover, the IHC staining assay for GPX4 showed that IPA but not tryptophan supplementation could significantly elevate the GPX4 expression in heart tissue after MI/R in the CSDS mice (Fig. 6K). We also observed significantly decreased 4-HNE and ROS levels after IPA supplementation in the CSDS + IPA + MI/R group compared to the CSDS + Trp + MI/R group (Fig. 6L and S5F). Three weeks after IPA or tryptophan supplementation, it was indicated that tryptophan supplementation did not yield a significant improvement in myocardial fibrosis and cardiac remodeling in CSDS mice after MI/R, in contrast to IPA supplementation, which demonstrated a notable effect (Fig. 6M and N). Collectively, our results suggested that IPA treatment significantly alleviates cardiac dysfunction and decreases ferroptosis post-MI/R in CSDS mice, whereas direct tryptophan supplementation does not. Over time, IPA supplementation improved heart remodeling and reduced myocardial fibrosis in mice. This observation further suggests that the increased susceptibility of CSDS mice to MI/R injury is primarily attributable to the impaired ability to metabolize tryptophan into the crucial metabolite IPA.

2.7. IPA deficiency contributes to the advanced progression of MI/R in vivo

Based on prior findings, it has been identified that disruptions in tryptophan metabolism may contribute to the exacerbation of cardiac damage following MI/R in mice experiencing depression. Furthermore, supplementation with IPA appears to mitigate this effect. To investigate whether IPA mediates the enhanced MI/R impairment associated with tryptophan metabolism disorder in depressed mice, we have designed the following experiments. 8-week-old C57BL/6 mice were fed a tryptophan-depleted diet (TDD), TDD supplemented with tryptophan (TDD + Trp), TDD + Trp with antibiotic administration (TDD + Trp + ABX), or TDD + Trp + ABX supplemented with IPA (TDD + Trp + ABX + IPA) (Fig. 7A). TDD feeding led to a larger myocardial infarct size and poorer cardiac function after MI/R injury (Fig. 7B and C). The CK-MB levels was significantly increased in TDD and TDD + Trp + ABX groups after MI/R (Fig. S6F). Treatment with TDD and antibiotic without Trp or IPA induced a significant decrease in the relative expression levels of GPX4, SLC7A11, FTH, and NRF2 in mice compared to the groups with Trp or IPA supplementation after MI/R (Fig. 7D). Moreover, IL-1β, IL-6, ACSL4, and PTGS-2 mRNA expressions were upregulated and that of GPX4 was downregulated in the TDD + MI/R group, which was restored by IPA supplementation (Figs. S6A–S6E). Mice in the TDD and TDD + Trp + ABX groups showed a remarkable decrease in serum IPA compared to the TDD + Trp and TDD + Trp + ABX + IPA groups after 4 weeks of treatment after MI/R (Fig. 7E). Of note, we found that serum IPA levels in mice positively correlated with EF% after MI/R (Fig. 7F). Furthermore, the iron contents increased in the TDD + MI/R group (Fig. 7G and H), and GSH levels in the heart and serum decreased in the TDD + MI/R group, as shown in Fig. 7I and J. In addition, we employed IHC staining after MI/R to evaluate whether the alleviation of cardiac injury by tryptophan or gut microbiota depleted is involved in the IPA supplementation. As expected, TDD + Trp and TDD + Trp + ABX + IPA groups showed increased GPX4 after MI/R (Fig. 7K). We also observed significantly increased 4-HNE and ROS levels after MI/R in the TDD and TDD + Trp + ABX groups compared to tryptophan or IPA supplementation (Fig. 7L and S6H). Three weeks following MI/R, we identified a significant increase in myocardial fibrosis and cardiac remodeling in mice with tryptophan deficiency and antibiotic-depleted intestinal microbiota. Conversely, supplementation with tryptophan and IPA markedly ameliorated these conditions (Fig. 7M and N). Antibiotic treatment (TDD + Trp + ABX) had almost the same effect as TDD, whereas the damage resulted by the inhibitory effect of the antibiotics on tryptophan metabolism was reversed by IPA supplementation. Taken together, these data indicate that reduced microbial IPA production contributes to the advanced progression of MI/R under conditions of

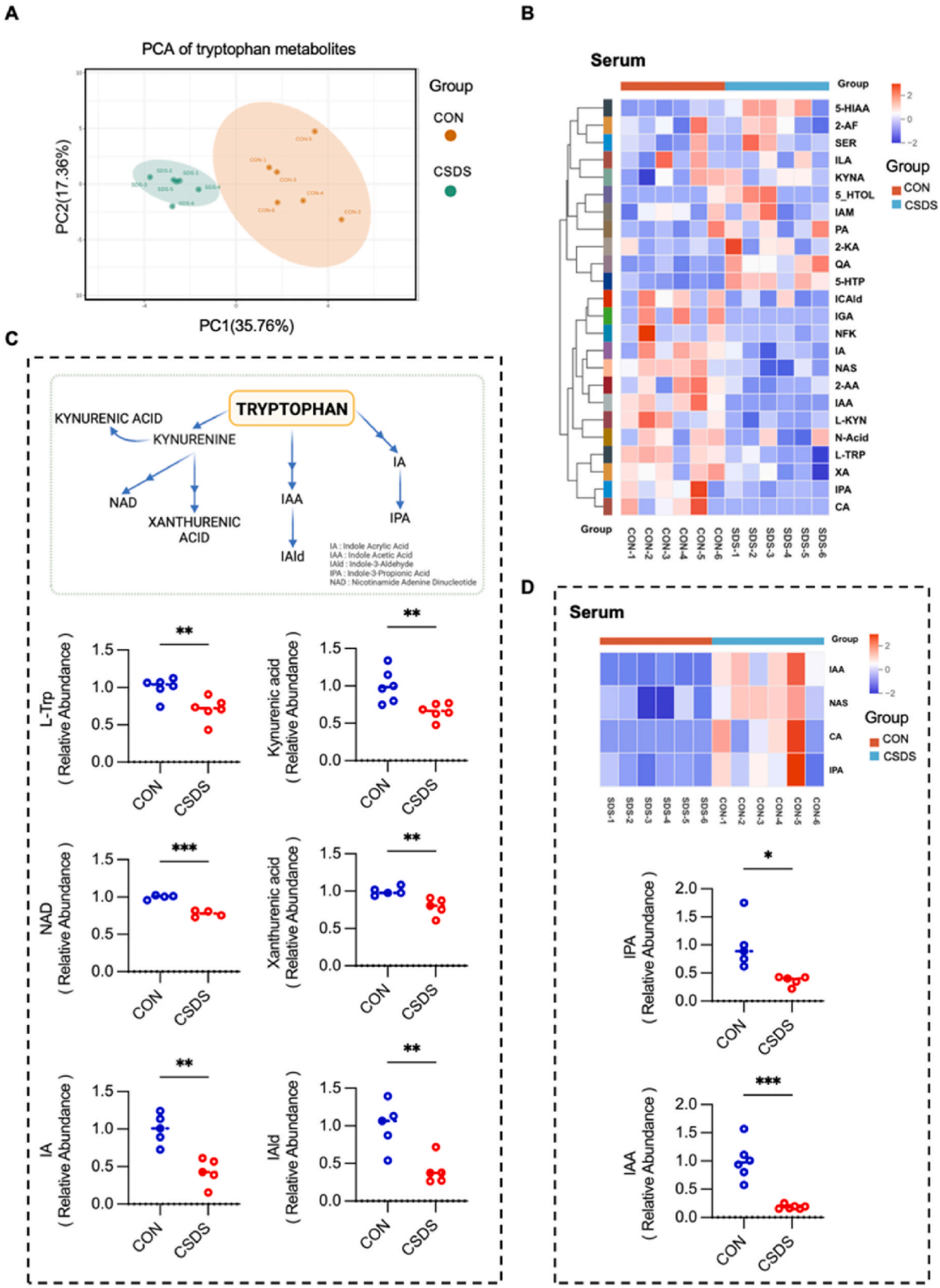

Fig. 5. Distinct tryptophan metabolites in CON and CSDS mice. (A) PCA of tryptophan metabolites in serum. (B) Hierarchical Cluster Analysis (HCA) of tryptophan metabolites in serum. (C) Relative abundance of tryptophan related metabolites in serum. (D) Differential metabolite clustering heat map. Data are expressed as mean ± SE, n = 4–6, ns, no significance, $*p < 0.05$, $**p < 0.01$, $***p < 0.001$.

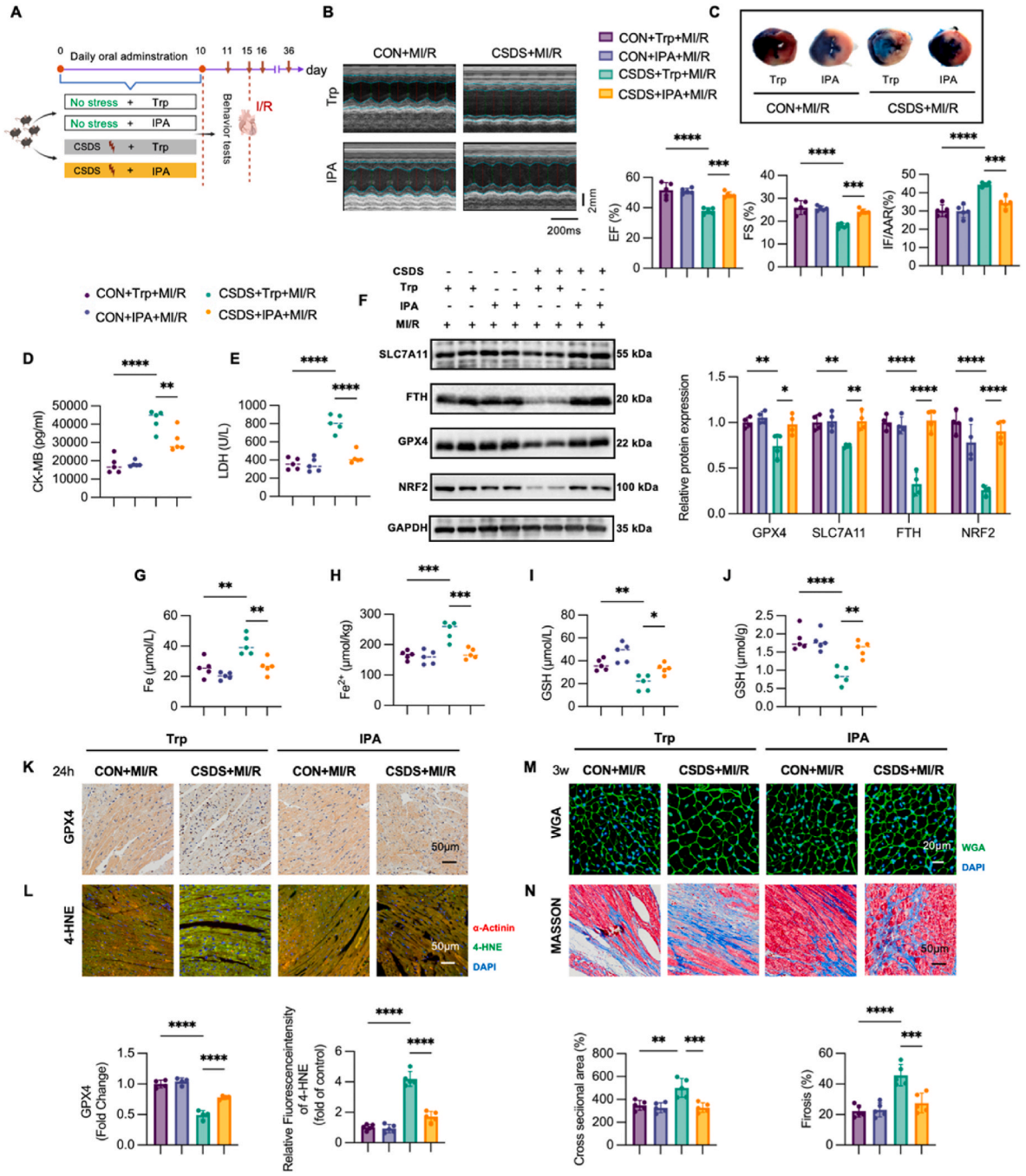

Fig. 6. Indole-3-propionic acid (IPA) supplementation rescued cardiac dysfunction and cardiac remodeling post-MI/R in CSDS mice resulted by impaired tryptophan metabolism. (A) Experimental design. (B) Transthoracic echocardiography of mice. (C) TTC staining of heart tissue. (D) The CK-MB levels in serum. (E) The LDH levels in serum. (F) Relative proteins expression of ferroptosis in heart tissue. (G–H) Total and ferrous iron levels in serum and heart tissue. (I–J) GSH levels in serum and heart tissue. (K) The immunohistochemistry staining of GPX4 in heart tissue. (L) The immunofluorescent staining of 4-HNE in heart tissue. (M) WGA staining of heart tissues. (N) Masson staining of heart tissues. Data are expressed as mean ± SE, n = 3–6, ns, no significance, $^{*}p < 0.05$, $^{**}p < 0.01$, $^{***}p < 0.001$, $^{****}p < 0.0001$.

depression and serum IPA levels positively correlated with EF% after MI/R in mice.

2.8. IPA inhibits myocardial ferroptosis and improves oxidative stress induced by oxygen-glucose deprivation/reoxygenation (OGD/R) in vitro through activating NRF2

We further investigated the mechanism by which IPA exert its protective effects in MI/R injury in vitro. As expected, IPA decreased the ferroptosis of H9c2 induced by OGD/R, as indicated by a reduction in ROS level and FerroOrange staining (Fig. 8A and B). Furthermore, IPA upregulated the protein expression of GPX4, SLC7A11, FTH, and NRF2 in H9c2 after OGD/R (Fig. 8C). Similar protective role of IPA was also observed in HL-1 cells (Fig. 8D–F). This suggests that the NRF2/System xc-/GPX4 axis is activated. IPA also decreased H9c2 and HL-1 ferroptosis induced by OGD/R as indicated by the reduction in ACSL4 and PTGS-2 mRNA expressions and increased GPX4 expression (Figs. S7C–S7E, Figs. S7H–S7J). We then analyzed whether NRF2 mediated the protective effects of IPA on ferroptosis by using siRNA targeting NRF2. Our findings indicate that IPA enhances NRF2

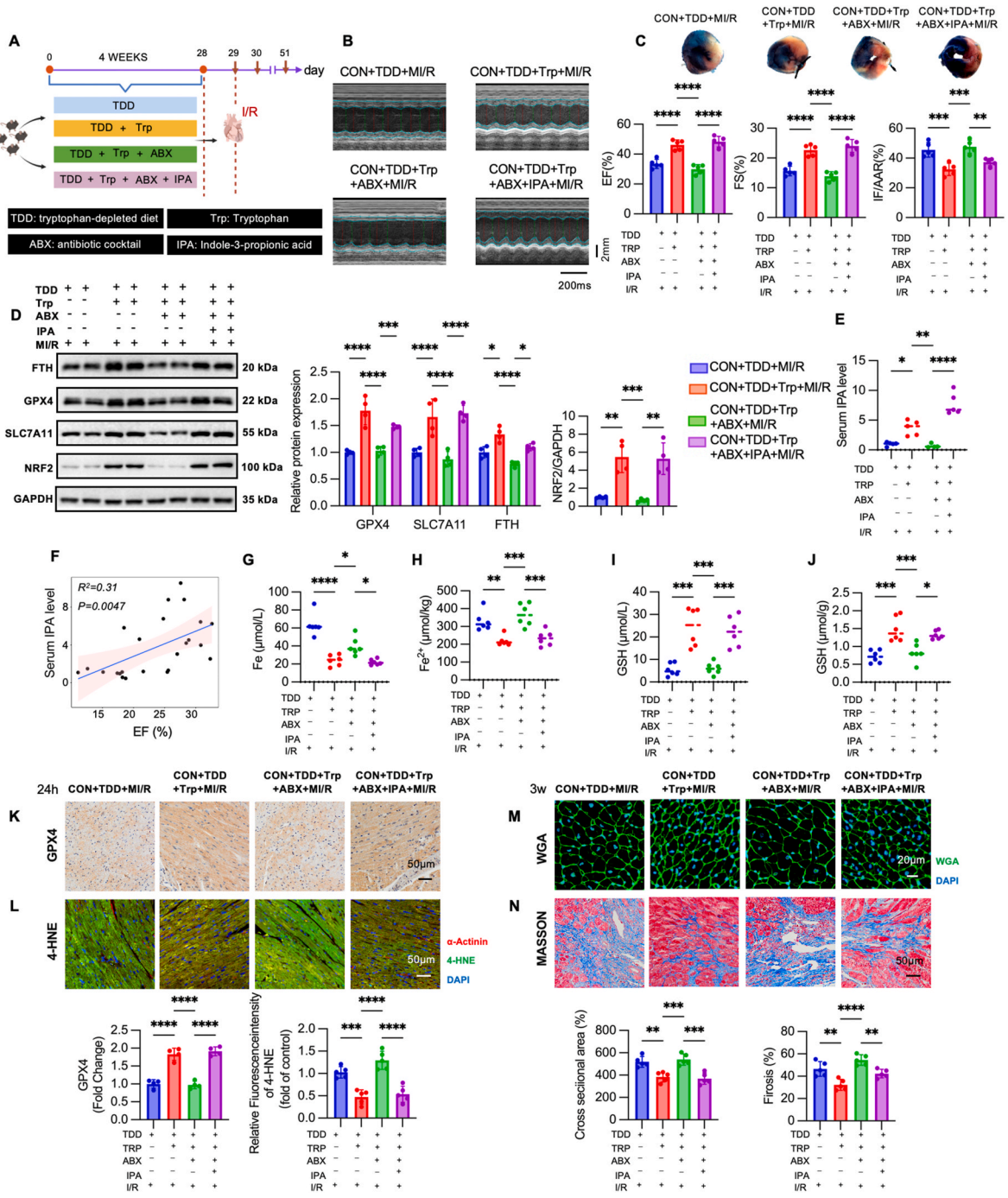

Fig. 7. IPA deficiency contributes to the advanced progression of MI/R. (A) Experimental design. (B) Transthoracic echocardiography of mice. (C) TTC staining of heart tissue. (D) Relative proteins expression of ferroptosis in heart tissue. (E) The IPA level in serum. (F) Correlations between IPA level in serum with the EF (%). (G–H) Total and ferrous iron levels in serum and heart tissue. (I–J) GSH levels in serum and heart tissue. (K) The immunohistochemistry staining of GPX4 protein in heart tissue. (L) The immunofluorescent staining of 4-HNE protein in heart tissue. (M) WGA staining of heart tissues. (N) Masson staining of heart tissues. Data are expressed as mean ± SE, n = 3–30, ns, no significance, *$p < 0.05$, **$p < 0.01$, ***$p < 0.001$, ****$p < 0.0001$.

expression, and the inhibition of NRF2 by siRNA abrogates the protective effects of IPA against oxidative stress (Fig. 8G–I). Overall, these results identified the potential role of IPA in mitigating the oxidative damage associated with MI/R injury through NRF2/System xc-/GPX4 axis in vitro.

3. Discussion

The contribution of gut microbiota and their metabolites to health and disease susceptibility has been increasingly recognized. In this study, we found that depression exacerbated post-MI/R cardiac damage in a mouse model of depression and induced significant alterations in the gut microbial richness and community structure. Furthermore, fecal microbial transplantation in germ-free mice confirmed the mediating effect of gut microbiota in the decreased cardiac function in CSDS mice after MI/R injury. We also found that impaired tryptophan metabolism resulted in decreased levels of a series of metabolites, especially IPA, in depressed mice. Meanwhile, we identified a positive correlation between serum IPA levels and cardiac function following MI/R. In additional, we observed that decreased gut microbiome-derived IPA could

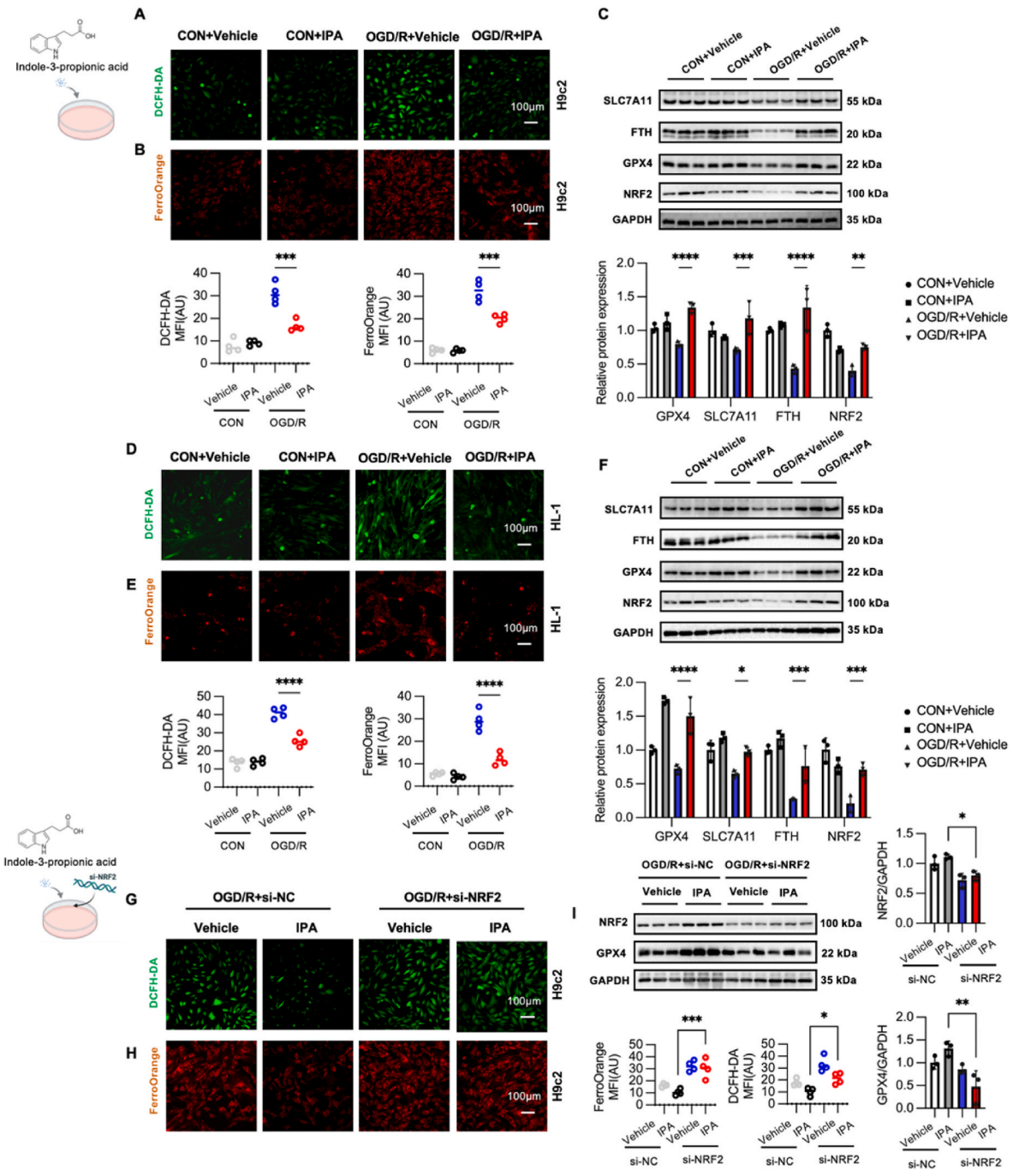

Fig. 8. IPA inhibits myocardial ferroptosis and improves oxidative stress induced by oxygen-glucose deprivation/reoxygenation (OGD/R) in vitro via nuclear factor erythroid 2-related factor 2 (NRF2). (A) Intracellular DCFH-DA level and quantitative analysis of DCFH-DA fluorescence in H9c2 cells. (B) FerroOrange staining and quantitative analysis of FerroOrange fluorescence in H9c2 cells. (C) Relative proteins expression of ferroptosis in H9c2 cells. (D) Intracellular DCFH-DA level and quantitative analysis of reactive oxygen species (ROS) fluorescence in H9c2 cells. (E) FerroOrange staining and quantitative analysis of FerroOrange fluorescence in H9c2 cells. (F) Relative proteins expression of ferroptosis in H9c2 cells. (G) Intracellular DCFH-DA level and quantitative analysis of DCFH-DA fluorescence in H9c2 cells. (H) FerroOrange staining and quantitative analysis of FerroOrange fluorescence in H9c2 cells. (I) Relative proteins expression of NRF2 and GPX4 in H9c2 cells. MFI: Mean fluorescence intensity. Data are expressed as mean ± SE, n = 3, ns, no significance, $*p < 0.05$, $**p < 0.01$, $***p < 0.001$, $****p < 0.0001$.

mediate the exacerbation of MI/R injury following depression both in vivo and in vitro. Mechanistically, IPA acted as a novel protector against ferroptosis via the NRF2/System xc-/GPX4 axis in MI/R injury. Our study provides a novel brain-gut-heart axis dependent mechanism into the relationship between depression and cardiovascular disease, offering the therapeutic potential of IPA for CVD patients with depression. This is particularly important for the patients experiencing comorbid CVD and depression, who experience a poorer prognosis than their counterparts without depression. Furthermore, these findings are expected to greatly contribute to the advancing field of the physiological role of the gut microbiome.

Recent years have witnessed an increase in gut microbiota as a major topic of research interest in biology. Numerous previous studies focused on the effects of the "microbiota-gut-brain axis" [9,11,42,43]. It was demonstrated that alterations in the gut microbiota can induce depression-like behaviors in mouse models and influence the

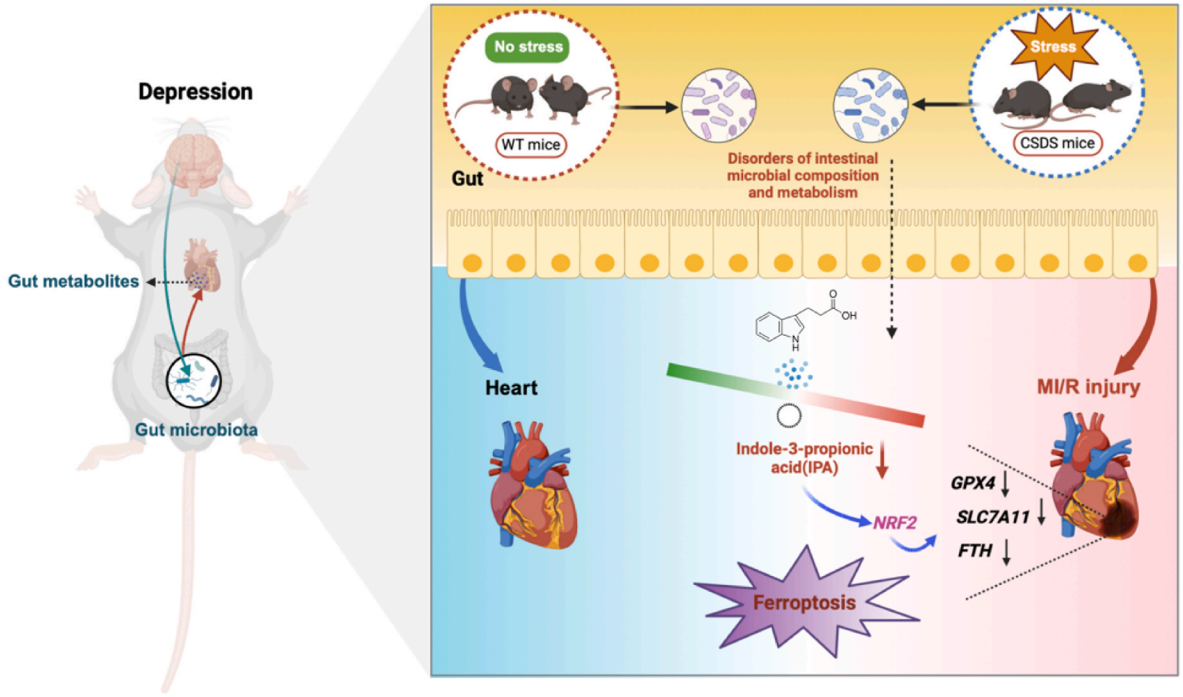

Fig. 9. Schematic illustration of the mechanism of decreased gut microbiome-derived indole-3-propionic acid mediates the exacerbation of myocardial ischemia/reperfusion injury following depression via the brain-gut-heart axis. Depression changed gut microbial richness and community structure, resulting in impaired tryptophan metabolism. The disorders of gut microbial composition and metabolism led to decreased levels of a series of metabolites, including IPA. Decreased serum IPA, which could protect cardiomyocytes against ferroptosis post MI/R via NRF2/System xc-/GPX4 axis, mediated the detrimental influence of depression on MI/R.

pathophysiology of depression in human patients [13,44–47]. Therefore, this study used ABX and FMT to explore the mediating effect of the gut microbiota in depressed mice and to verify whether this microbiota plays a key role in the exacerbation of MI/R by depression. Given that long-term intervention (≥2 weeks) with mixed antibiotics can lead to depression-like behavior in mice [48], a short-term (7 days) antibiotic intervention was used to deplete their gastrointestinal microbiota, as well as preventing antibiotic-induced depression in mice in our study. Our results indicated that transplanting feces from depressed mice but not control mice aggravated MI/R in recipient mice, suggesting that depressed mice have altered gut microbiota, which in turn affects the susceptibility to MI/R. It's also well established that a diverse, well-balanced gut microbiota, mainly composed of Firmicutes, Bacteroidetes, Actinobacteria, Proteobacteria, Fusobacteria, and Verrucomicrobia, is crucial for human health [49,50]. In our work, we found that CSDS mice showed changed community richness and diversity of gut microbial based on β diversity. At the phylum level, the Firmicutes/Bacteroidetes ratio, which was considered an indicator of intestinal disorders, was decreased in the CSDS mice. At the genus level, the abundance of Bacteroides and Klebsiella were reported to be significantly increased in the CUMS group [51]. In our study, it was found that *g_Bifidobacterium, g_Bacteroides, and Lactobacillus* spp. decreased in mice with depression. *Bifidobacterium* and *Lactobacillus* have been previously documented to mitigate obesity and inflammation, enhance depressive symptoms, and facilitate the development and regeneration of the intestinal epithelium, which is consistent with our data [52–54]. Our findings indicated that the gut microbiota in mice with depression is significantly modified in a manner that predisposes them to disease.

The gut microbiome functions analogously to an endocrine organ, producing bioactive metabolites including short-chain fatty acids and bile acids, which can significantly influence host physiology [55]. Previous studies have found that MDD is associated with disturbances in the peripheral and central metabolites [56–58]. It was reported that perturbations in the gut microbiome are strongly correlated with modifications in fecal metabolites, particularly tryptophan, and the abundance of four metabolic pathways in the intestinal microbiota associated with tryptophan biosynthesis and metabolism is significantly reduced in patients with MDD [59,60]. In our study, we found that the tryptophan metabolic pathway was significantly inhibited in the CSDS mice, indicating the key role of tryptophan metabolism. Recent studies have shown that the gut microbiota is also closely related to the pathogenesis of coronary heart disease and depression, primarily through multilevel regulation of the microbiota-gut-brain axis, encompassing inflammatory responses, chronic inflammation, and metabolites [61]. Tryptophan, an essential and only aromatic amino acid with an indole structure, is an important metabolite in the crosstalk between the gut microbiota and host [18]. Tryptophan metabolites, as ligands, can activate AHR signaling in various pathological states, such as inflammation, oxidative stress injury, and CVD [62]. Therefore, tryptophan, or its metabolites, is speculated to play a key role in depression and CVD and may even act as a "bridge." Interestingly, we found that tryptophan administration significantly improved cardiac function in mice without depression but had no effect on chronic stress-induced depression. The reason for this phenomenon may be that CSDS mice cannot directly use tryptophan owing to changes in the gut microbiota, especially those related to tryptophan metabolism. The metabolism of tryptophan within the gastrointestinal tract encompasses the direct conversion of tryptophan by intestinal microbiota into various compounds, such as indole and its derivatives [18]. For example, Clostridium converts tryptophan to tryptamine, indolylactic acid (ILA), and IPA; *Peptostreptococcus* spp., including P. russellii, P. anaerobius and P. stomatis, can convert tryptophan to indoleacrylate (IA) and IPA; The *Lactobacillus* spp. converts tryptophan to indolaldehyde (IAld) and ILA through aromatic amino acid aminotransferase (ArAT) and indole lactate dehydrogenase (ILDH) [63–65]. Consistent with our expectations, several gut microbiota species involved in tryptophan metabolism, such as *Peptostreptococcus* spp., *Lactobacillus* spp., *Bifidobacterium* spp., and *Parabacteroides* spp. were reduced in CSDS-treated mice. This further confirms that psychological stress influences the pathophysiological conditions of multiple host systems and organs through its effects on intestinal microbiota.

Metabolism is a key pathway through which depression affects the gut microbiota via the brain-gut axis, particularly through direct changes in the levels of key metabolites and indirect alterations in circulating serum metabolites [66]. Therefore, we used LC-MS/MS to detect tryptophan metabolites in mice with CSDS-induced depression. We quantified 31 substances related to tryptophan metabolic pathways, and our observations indicated a reduction in several tryptophan metabolites, such as L-tryptophan, kynurenic acid, IAA, and IPA, in CSDS-induced mice. This suggests that depression affects host health by modifying the composition of gut microbiota, consequently influencing related metabolic pathways and metabolites.

IPA is a metabolite derived solely from dietary tryptophan, which can be absorbed from the gut into the circulation and shows a high degree of inter-individual variation. In recent years, IPA has attracted researcher's attention as a novel protective factor for intestinal and metabolic diseases [18,67,68]. For example, microbiota-derived IPA can alleviate intestinal inflammation and regulate gut microbiota [67]. Moreover, circulating IPA concentrations are inversely associated with type 2 diabetes risk [68]. An integrative analysis of the intestinal microbiota and metabolome revealed a significant reduction in IPA levels in patients with coronary artery disease (CAD). Furthermore, circulating IPA concentrations were inversely correlated with the risk and severity of atherosclerotic cardiovascular disease in a separate cohort [21]. Moreover, dietary supplementation with IPA exerted protective and therapeutic effects in mouse models of heart failure with preserved ejection fractions [20]. In addition, IPA significantly reduced the concentration of pro-inflammatory TNF-α in microglia, exerting a protective role on nerves [69]. However, the role of the IPA in depression-exacerbated MI/R injury remains unknown. In this study, we found that plasma and serum IPA was significantly decreased in CSDS-induced mice and that serum IPA levels showed a significant positive correlation with EF% after MI/R. In our study, administration of IPA to CSDS mice resulted in a significant reduction in cardiac damage. To investigate the underlying mechanism by which IPA mitigates MI/R injury, we conducted in vitro experiments in which IPA was administered to H9C2 and HL-1 cell lines and resulted in protective effects in hypoxia and reoxygenation models. These findings suggested that the cardioprotective effects of IPA can be attributed to its direct action on cardiomyocytes. IPA may be a potential intervening target for CVD patients with depression.

Accumulating evidence indicates that ferroptosis plays a key role in the pathogenesis and progression of various cardiovascular diseases, including MI/R [70]. In our study, IPA consistently suppressed ferroptosis in cardiomyocytes and enhanced the expression of GPX4, a key regulator of ferroptosis. IPA supplementation increased the concentration of GSH and enhanced the expression of SLC7A11, which, in turn, inhibited ferroptosis. Lipid peroxidation is an important hallmark of ferroptosis [71]. IPA decreases OGD/R-induced oxidative stress in HL-1 and H9c2 cells, consistent with a previously reported role of IPA in oxidative stress [72]. Thus, our findings suggested a conserved molecular mechanism by which IPA inhibits ferroptosis in cardiomyocytes. However, the specific mechanism by which IPA exerts its protective function on cardiomyocytes was not studied in this work.

Tryptophan metabolites, such as tryptamine, methylindole, IAA, IA, IAld, and ILA, serve as ligands for aryl hydrocarbon receptors (AHR) [73–75]. AHR is a transcription factor extensively expressed by immune system cells, and numerous studies have demonstrated that AHR activation modulates both innate and adaptive immune responses in a ligand-specific manner [76]. For instance, indole-induced AHR activation may represent a mechanism through which the microbiome facilitates mucosal homeostasis [73]. Studies have indicated that IPA may mitigate metabolic disorders and reduce inflammation via its interaction with the AHR [77,78]. Recent studies indicate that the administration of IPA significantly mitigates bone loss in ovariectomy (OVX)-induced postmenopausal osteoporosis in mice by enhancing intestinal barrier integrity through an AHR-dependent mechanism [79]. Additionally, IPA was found to enhance cardiac function via the AHR/NF-κB/NLRP3 axis in animal septic cardiomyopathy model [80].

Besides AHR, recent research has demonstrated that commensal bacteria are capable of producing molecules that mimic ligands of G-protein coupled receptors (GPCRs) [81,82]. Research has demonstrated that the gut GPR35 plays a role in the microbial-brain metabolic pathway, influencing neuronal plasticity and depressive behavior in mice [37]. Furthermore, an additional study demonstrated that IAA and IPA exhibit neuroprotective effects in mice subjected to D-galactose-induced aging by activating the GPR30/AMPK/SIRT1 signaling pathway [72]. Additionally, pharmacological activation of the exogenous inductive nuclear receptors, pregnane-X receptor (PXR) and constitutive androstane receptor (CAR), is recognized for enhancing drug metabolism and mitigating inflammation [83]. A diverse array of bacterial metabolites exist in the colonic lumen, including the tryptophan derivative IPA, as well as the secondary bile acids deoxycholic acid (DCA) and lithocholic acid (LCA), have been shown to activate the PXR and the CAR, thereby influencing the expression of their target genes [84,85]. These studies indicate that tryptophan metabolites may influence the PXR and CAR signaling pathways; however, further research is required to elucidate this relationship. Collectively, tryptophan metabolites could function as ligands for a couple of receptors, including AHR, GPCRs, and PXR. This offers novel insights into the mechanisms by which IPA exerts its protective function on cardiomyocytes. Therefore, in the future, a series of experiments exploring the potential roles of AHR, GPCRs, and PXR will be performed to fully understanding the therapeutic potential of IPA.

In this study, we observed that supplementation with IPA demonstrated a capacity to mitigate cardiac damage and enhance cardiac function by attenuating ferroptosis and long-term cardiac fibrosis. However, the potential indirect cardioprotective effects of IPA through the alleviation of depressive symptoms remain to be investigated. Of note, numerous studies have demonstrated a correlation between tryptophan metabolites produced by gut microbiota and the onset and progression of depression. Furthermore, supplementation with these metabolites has been shown to alleviate depressive symptoms and the social and cognitive deficits in rodents [86,87]. Recent findings indicate the potential antidepressant effects of psychobiotic-derived ILA through the activation of AHR signaling pathways [88].

Taken together, we identified IPA could be a key microbially produced tryptophan metabolite of the detrimental effects of depression on MI/R. IPA exert its protective functions on cardiomyocytes ferroptosis through NRF2/System xc-/GPX4 axis in CSDS mice after MI/R, thus alleviating the development of MI/R. These findings are clinically relevant as they may form the basis of intervention strategies aimed at mitigating the deterioration of cardiac function in patients experiencing depression following MI/R using the microbiome and gut microbiota-derived IPA.

4. Conclusion

Our findings provide new insights into the role of the gut microbiota and IPA in depression and CVD, forming the basis of intervention strategies aimed at mitigating the deterioration of cardiac function in patients experiencing depression following MI/R. In future clinical practice, microbiota-targeted therapies or IPA supplementation may serve as innovative therapeutic strategies for patients suffering from depression and cardiovascular disease.

5. Limitations

Some limitations of this study need to be mentioned. This study did not incorporate clinical data, and alternative depression models were not explored. Furthermore, the specific receptor by which IPA exerts its effects on cardiomyocytes remains unclarified.

6. Materials and methods

6.1. Animals and procedures

All animal procedures were approved by the Animal Experiment Welfare and Ethics Committee of Air Force Military Medical University (NO.20241450). Male C57BL/6 mice aged 8–10 weeks were procured from Air Force Military University (AFMU, Shaanxi, China), while male CD-1 mice aged 4–6 months were obtained from Beijing Vital River Laboratory Animal Technology Co., Ltd. (Beijing, China). Both groups were housed in the specific pathogen-free (SPF) laboratory animal facility of AFMU (Xi'an, China). The mice were maintained under a 12-h light/dark cycle at a temperature of 25 °C and were provided ad libitum access to commercially available rodent chow, sterilized using Cobalt-60, and tap water, sterilized at high temperatures, prior to the commencement of the experiments. Randomized grouping was implemented, with the same cohort of mice co-housed at a density of five animals per cage. All experimental protocols received approval from the Animal Care and Use Committee of the AFMU (Xi'an, China) and adhered to the guidelines set forth in the National Research Council's Guide for the Care and Use of Laboratory Animals in China.

Social defeat stress was induced as previously reported, with minor modifications [89,90]. Before performing the social defeat experiments, CD-1 retired breeder mice were singly housed, allowing habituation for a minimum of 7 days prior to screening. Appropriate CD-1 aggressive mice were selected from the three-day screening process to meet the social defeat criteria [91]. CD-1 mice exhibiting extremely aggressive behavior or no aggression were excluded from the experiments. Only mice showing aggression within 1 min and persistent aggressive intentions were used in the social defeat sessions [91]. An intruder mouse (C57BL/6 mice) was introduced into the home cage of a CD-1 resident mouse for 5–10 min to induce social defeat stress, with the intruder exhibiting apparent freezing behavior, a submissive posture, or climbing during this time. A transparent partition was subsequently used to separate the intruder and resident mice; however, the intruder remained in olfactory, visual, and auditory contact with the resident mice for 24 h. This process was repeated for 10 days, and C57BL/6 mice were attacked by different CD-1 mice every day, eventually exhibiting depression-like behavior.

6.2. Behavioral tests

6.2.1. Social interaction test (SIT)

A SIT was conducted to assess the social behavior of C57BL/6 mice [91]. The SIT was administered 24 h following the final exposure to social defeat stress. During the SIT, CD-1 mice were entirely unfamiliar to the C57BL/6 mice under examination. The test involved placing each mouse individually in a thoroughly cleaned open-field apparatus. In the initial 2.5-min session, referred to as the "no target" phase, each C57BL/6 mouse was allowed to freely explore the arena, which contained an empty cage to facilitate visual, olfactory, and auditory stimuli. During the second 2.5-min session, referred to as the "target" session, the previously empty cage was substituted with a cage containing a target, specifically an unfamiliar aggressive CD-1 mouse, for each defeated C57BL/6 mouse. The duration of time that C57BL/6 mice spent within the interaction zone, defined as the 10 cm area surrounding the cage, was recorded across two sessions. Consequently, the social interaction ratio was calculated as the proportion of time spent in the interaction zone with the target CD-1 mouse to the time spent in the interaction zone without a target [91].

6.2.2. Tail suspension test (TST)

The TST is widely used to assess depression-like behavior in mice [92]. The C57BL/6 mouse was suspended from the tail, such that it could not touch the ground (the distance from the ground to the head of the mouse was approximately 50 cm). The experiment lasted for 6 min, and each mouse was allowed to adapt for 2 min after the suspension. The time at which C57BL/6 mice ceased struggling and remained immobile was monitored and recorded [92].

6.2.3. Forced swimming test (FST)

The FST is a highly reliable test for evaluating depression-like behavioral states [92,93]. The mice were individually placed into a clear glass cylinder (high enough to prevent the mice escaping) filled with 30 cm of water (maintained at 24 ± 1 °C). Similar to the TST, each mouse was allowed to adapt for 2 min. Immobility time was defined as the immobile time spent by the mice floating in the water with no active movements but with movements necessary to keep their heads above water [89,92].

6.2.4. Sucrose preference test (SPT)

The SPT is commonly used to observe anhedonic-like behavior in mice [94]. All mice were deprived of food and water for 12 h before SPT. The mice were subsequently given two standard drinking bottles, one containing 1 % sucrose and the other containing tap water, for 24 h. The positions of the two bottles were switched every 6 h to avoid side preference. Sucrose and water intake were measured after the SPT, and the sucrose preference rate was presented as a percentage of sucrose intake/sucrose intake plus water intake [92,94].

6.2.5. Open-field test (OFT)

The OFT was performed to evaluate the locomotor and exploratory behaviors of mice [95]. The OFT was performed in a box (50 × 50 × 50 cm). Each mouse was placed in a corner at the start of the test and was recorded for 5 min using a camera located above the box. The device was cleaned with 75 % alcohol after each trial. A tracking system with an automated analysis system recorded the number of entries into the center zone, the time spent in the center zone, and the total distance traveled (SMART 3.0, Panlab S.L.U., Spain). The center area of the open-field apparatus was 25 % of the total area (a square of approximately 25 × 25 cm) [92].

6.3. Myocardial ischemia/reperfusion (MI/R)

Mice were anesthetized with 2 % isoflurane, the chest cavity was opened at the fourth intercostal space, and the pericardium was excised. Subsequently, a 7-0 silk ligature was positioned distal to the left atrial appendage, spanning the sternal portion of the left ventricle, which included the left anterior descending coronary artery, for 30 min. The sutures were subsequently released to allow reperfusion of the ischemic area. The sham-operated mice underwent the same surgery without tying the left anterior descending coronary artery. The animals were returned to their feeding cages after recovery [32].

6.4. Echocardiography

Transthoracic echocardiography was employed to assess cardiac function, specifically evaluating the left ventricular ejection fraction (EF %) and fractional shortening (FS%). The echocardiographic assessments were conducted utilizing the Visual Sonics Vevo 2100 system (Visual Sonics Inc., Toronto, Ontario, Canada), equipped with a scan head operating at a central frequency of 30 MHz. M-mode images were acquired through the parasternal short-axis view at the level of the papillary muscles. Each mouse underwent anesthesia with 2 % isoflurane, and measurements were performed a minimum of three times per subject.

6.5. Infarct size measurement

To determine the myocardial infarct size, 1 % Evans blue dye (Sigma) was perfused into the heart through the aorta after the LAD artery was tied to the previous location. The hearts were then frozen and cut into

1–2 mm slices. Next, the slices were incubated in 1 % 2,3,5-triphenyl tetrazolium chloride solution (Sigma) for 15–20 min at 37 °C. After photography, the images were analyzed using ImageJ software. The infarct area (pale area) and AAR (pale area plus pink area) were determined by planimetry using ImageJ. The infarct size was calculated as the infarct area divided by the AAR [32].

6.6. Antibiotic treatment and fecal microbiota transplantation

A combination of antibiotics, including ampicillin (0.1 mg mL^{-1} d^{-1}) (A9518, Sigma–Aldrich, USA), neomycin (0.1 mg mL^{-1} d^{-1}) (N6386, Sigma–Aldrich, USA), and metronidazole (0.1 mg mL^{-1} d^{-1}) (M3761, Sigma–Aldrich, USA), was mixed with drinking water and administered to mice for 7 days to deplete their gastrointestinal microbiota [96]. Animals that received the antibiotic cocktail were referred to as ABX mice.

6.7. Fecal microbiome transplantation

Regarding microbiota transplantation, endpoint-mice fecal samples (100 mg per mice) collected under sterile conditions were resuspended with pre-cooled PBS and centrifuged at 1000 rpm for 5 min at 4 °C. Next, the supernatant was removed, the sample was centrifuged at 8000 rpm for 10 min at 4 °C, and the supernatant was discarded. Subsequently, glycerin (25 %) was added before storage at – 80 °C [96]. Mice drank the antibiotic cocktail for 7 days and were then orally inoculated with the mixture (200 μl for each mouse) for 2 weeks.

6.8. Metagenomics

At the endpoint of the experiments, one mouse was placed in a cage, and its feces (100 mg per mice) were collected under sterile conditions, frozen using liquid nitrogen, and stored at – 80 °C. Library preparation, sequencing, and operational taxonomic unit table generation were performed using the STANDARD GROUP (Qingdao, China). Briefly, microbial DNA was extracted from colonic contents using the PowerSoil® DNA Isolation kit (Mobio, U.S.), according to the manufacturer's instructions. The final DNA concentration and purity were determined using a NanoDrop 2000 UV–vis spectrophotometer (Thermo Scientific, Wilmington, USA), and DNA quality was evaluated by agarose gel electrophoresis. PCoA was performed to visually evaluate gut microbial differences. LDA effect size (LEfSe) analysis was used to identify differentially expressed bacterial taxa between the groups. In this project, the microbial metabolites were quantified using a liquid chromatograph mass spectrometer (LC-MS) system (Thermo, Vanquish, Q Exactive HF).

6.9. Metabolites treatment

Regarding tryptophan treatment (Sigma), 6–8-week-old male mice were treated with tryptophan (2 g/kg body weight [BW]) individually dissolved in autoclaved water for 10 days. To evaluate the effect of IPA (Sigma, IPA, 220027), 6–8-week-old male mice were treated with IPA (20 mg/kg BW) or vehicle (PBS) by oral gavage daily for 10 days before MI/R injury. To further investigate the role of gut microbiota in tryptophan metabolism, 6–8-week-old male mice fed the chow diet were randomly assigned into four groups: tryptophan-depleted diet (TDD); TDD supplemented with tryptophan (2 g/kg BW, TDD + Trp); TDD + Trp with antibiotic cocktail administration (TDD + Trp + ABX); or TDD + Trp + ABX supplemented with IPA (20 mg/kg BW, TDD + Trp + ABX + IPA), as previously described [21,22].

6.10. Detection of tryptophan and its metabolites

The analysis of IPA and other targeted tryptophan metabolites was conducted using LC-MS/MS. Following thawing, a 50 μL aliquot of the sample was extracted with 250 μL of methanol. Subsequently, 10 μL of a mixed internal standards (IS) solution, at a concentration of 250 ng/mL, was added to the extract to serve as an internal standard for quantification. The extract was then vortexed for 3 min, refrigerated at −20 °C for 30 min, and centrifuged at 12,000 rpm for 10 min at 4 °C. A 150 μL portion of the supernatant was collected and subjected to a second centrifugation at 12,000 rpm for 5 min at 4 °C. Finally, 100 μL of the supernatant was transferred for subsequent LC-MS analysis. The sample extracts were subjected to analysis using the LC-ESI-MS/MS system, specifically the UPLC, ExionLC™ AD (available at https://sciex.com.cn), and the QTRAP® 6500+ System (available at https://sciex.com). The analytical parameters were defined as follows: the high-performance liquid chromatography (HPLC) column utilized was the Waters ACQUITY UPLC HSS T3 C18 (dimensions: 100 mm × 2.1 mm i.d., particle size: 1.8 μm). The solvent system comprised water with 0.1 % formic acid (Solvent A) and acetonitrile with 0.1 % formic acid (Solvent B). The gradient elution commenced at 10 % Solvent B from 0 to 1 min, increased linearly to 95 % Solvent B from 1 to 8 min, maintained at 95 % Solvent B from 8 to 9.5 min, and subsequently decreased back to 10 % Solvent B from 9.6 to 12 min. The flow rate was set at 0.35 mL/min, with a column temperature of 40 °C, and an injection volume of 5 μL. Linear ion trap (LIT) and triple quadrupole (QQQ) scans were conducted using a triple quadrupole-linear ion trap mass spectrometer (QTRAP), specifically the QTRAP® 6500+ LC-MS/MS System. This system was equipped with an ESI Turbo Ion-Spray interface and operated in both positive and negative ion modes, with control facilitated by Analyst 1.6.3 software (Sciex). The operational parameters for the ESI source were as follows: ion source type, ESI+/−; source temperature, 550 °C; ion spray voltage (IS), 5500 V for positive mode and −4500 V for negative mode; and curtain gas (CUR) pressure set at 35 psi. The analysis of tryptophan and its metabolites was conducted utilizing scheduled multiple reaction monitoring (MRM). Data acquisition was executed using Analyst 1.6.3 software (Sciex), while quantification of all metabolites was carried out with Multiquant 3.0.3 software (Sciex). Optimization of mass spectrometry parameters, including declustering potentials (DP) and collision energies (CE) for individual MRM transitions, was performed. A distinct set of MRM transitions was monitored for each elution period, corresponding to the metabolites eluted during that specific timeframe.

6.11. Immunofluorescence and immunohistochemistry

The mice were anesthetized with isoflurane at the end of the experiment. Brains were rapidly removed and fixed with paraformaldehyde for paraffin embedding. After dewaxing and rehydration, hippocampal brain sections (5 μm) were cut on a histotome. Brain tissues were blocked using QuickBlock™ Blocking Buffer (Beyotime, P0260) and incubated with Iba-1 (Wako, 1:500 dilution) overnight at 4 °C. The sections were then washed with PBS, probed with Alexa Fluor 555-conjugated (Abcam) secondary antibodies for 2 h at room temperature, and sealed with an antifade mounting medium (Servicebio, Wuhan, China). Microscopic fields were imaged using a 10 × confocal microscope (Olympus FV3000, Japan) [97].

Hearts were fixed, paraffin-embedded, and sectioned for immunofluorescence and immunohistochemistry. After dewaxing and rehydration, citrate buffer was used to restore the antigens, and the sections were incubated with Endogenous Peroxidase Blocking Buffer (Beyotime, P0100B). Next, peroxidase activity was inactivated, and tissues were blocked using QuickBlock™ Blocking Buffer and incubated with GPX4 (abcam, ab125066, 1:500 dilution), 4-HNE (Bioss, bs-6313R, 1:500 dilution), WGA (Sigma, 1:100 dilution) overnight at 4 °C. To visualize the target protein, for GPX4, a DAB solution was applied, followed by hematoxylin staining. The sections were dehydrated and sealed. For 4-HNE, probed with Alexa Fluor 488-conjugated (Abcam) secondary antibodies for 2 h at room temperature, and sealed with an antifade mounting medium (Servicebio, Wuhan, China). Microscopic fields were imaged using a 10 × confocal microscope (Olympus FV3000, Japan)

[33,98].

In heart tissue samples, intracellular ROS levels were quantified utilizing dihydroethidium (DHE) obtained from Beyotime (Shanghai, China). Tissue sections were incubated with 1 μmol/L DHE for 30 min at 37 °C.

Cardiac fibrosis was evaluated employing Masson's staining method. Mouse cardiac tissues were fixed and processed according to standard protocols for paraffin embedding. The sections underwent sequential incubation with iron hematoxylin stain, ponceau acid magenta, phosphomolybdate stain, and aniline blue dye. Following staining, the sections were mounted with glycerin, and 20 fields per section were analyzed at 200 × magnification.

6.12. Cell culture, treatment, and immunofluorescent staining

HL-1 and H9c2 cells were cultured as previously described [99,100]. Cells were cultured in DMEM (Pricella) supplemented with 10 % FBS and 1 % penicillin-streptomycin solution (Solarbio) and maintained at 37 °C with 5 % CO_2. Regarding metabolites treatment, cultured HL-1 and H9c2 cells were incubated with IPA (1 μM) 24 h before MI/R injury. To induce OGD/R (oxygen-glucose deprivation/reoxygenation), HL-1 and H9c2 cells were exposured to oxygen glucose deprivation for 3 h, the culture medium was replaced with serum- and glucose-containing DMEM, and the cells were transferred to a normal incubator for recovery for 3 h. ROS Assay Kit (Beyotime, S0033S) was used to detect ROS levels in the cells. FerroOrange (Dojindo, F374) acts as a fluorescent probe for fluorescence imaging of Fe^{2+} in living cells. All fields were viewed using a confocal microscope (Olympus FV3000, Japan).

6.13. LDH, CK-MB, iron content, and GSH level

LDH (Mouse Lactate Dehydrogenase (LDH) ELISA Kit, JONLNBI0), CK-MB (Mouse CKMB (Creatine Kinase MB Isoenzyme) ELISA Kit, Elabscience), Fe (Total Iron Colorimetric Assay Kit, Elabscience), Fe^{2+} (Ferrous Iron Colorimetric Assay Kit, Elabscience), and GSH (Total glutathione/oxidized glutathione assay kit, Jiancheng, China) levels in heart tissues and serum were quantified using commercially available kits. The assay process strictly followed the protocol provided by the reagent manufacturer.

6.14. RNA isolation and qPCR

At the end of the experiment, the mice were sacrificed. Heart tissues were microdissected, and total RNA was extracted using TRNzol Universal reagent (Tiangen, China, DP424) according to the manufacturer's protocol. One microgram of RNA was reverse transcribed into cDNA using the 5 × StarLighter Script RT all-In-one Mix (FOREVERSTAR, Beijing, China). qPCR was performed using the 2 × StarLighter HP SYBR Green qPCR Mix (FOREVERSTAR, Beijing, China). The amplification program included heating to 95 °C for 3 min, followed by 40 cycles of 95 °C for 10 s and 60 °C for 30 s. The primer pairs used were as follows: GAPDH forward: AGGTCGGTGTGAACGGATTTG, GAPDH reward: TGTAGACCATGTAGTTGAGGTCA, IL-1β forward: GCAACTGTTCCTGAACTCAACT, IL-1β reward: ATCTTTTGGGGTCCGTCAACT, IL-6 forward: TAGTCCTTCCTACCCCAATTTCC, IL-6 reward: TTGGTCCTTAGCCACTCCTTC, TNF-α forward: CCCTCACACTCAGATCATCTTCT, TNF-α reward: GCTACGACGTGGGCTACAG, GPX4 forward: GATGGAGCCCATTCCTGAACC, GPX4 reward: CCCTGTACTTATCCAGGCAGA, ACSL4 forward: CTCACCATTATATTGCTGCCTGT, ACSL4 reward: TCTCTTTGCCATAGCGTTTTTCT, PTGS-2 forward: TTCAACACACTCTATCACTGGC, PTGS-2 reward: AGAAGCGTTTGCGGTACTCAT. The relative gene expression data were calculated using the $2^{-\triangle\triangle Ct}$ method.

6.15. Western blot analysis

Mouse heart tissues were lysed using RIPA lysis buffer (Beyotime) supplemented with phenylmethylsulfonyl fluoride. An Enhanced BCA Protein Assay Kit (Beyotime) was used to determine protein concentrations. Equal quantities of total protein were separated using SDS-PAGE (12 %). Protein bands were transferred onto PVDF membranes (MILLIPORE®) using the wet tank transfer method. After blocking with 2 % BSA and washing with TBST, protein bands were blotted with primary antibodies at 4 °C overnight as follows: solute carrier family 7 member 11 (SLC7A11) (Proteintech, 26864-1-AP, 1:1000 dilution), GPX4 (Abcam, ab125066, 1:5000 dilution), FTH (Abcam, ab183781, 1:5000 dilution), NRF2 (ABclonal, 1:1000 dilution) and GAPDH (Servicebio, gb15004, 1:5000 dilution). After washing with TBST, the protein bands were blotted with a secondary antibody and monitored using ECL buffer (Engibody). Quantification of the Western Blots was performed using ImageJ.

6.16. Statistical analysis

All data are shown as the mean values ± standard error of the mean. Normal distribution was initially analyzed, and the Brown–Forsythe test was used to analyze the homogeneity of variance. Comparisons between the two groups were performed using an unpaired two-tailed Student's t-test. One-way analysis of variance followed by Tukey's post-hoc test was used to compare differences between more than two groups. Data that did not pass the normality test were analyzed using the Mann–Whitney *U* test or Kruskal–Wallis test, followed by Dunn's post hoc test. Statistical analyses were performed using the GraphPad Prism 10 software (GraphPad Software, La Jolla, CA, USA). All group numbers and detailed significance values are presented in the figures or legends.

CRediT authorship contribution statement

Xingdou Mu: Writing – review & editing, Writing – original draft, Methodology, Data curation, Conceptualization. **Lele Feng:** Writing – review & editing, Writing – original draft, Methodology, Data curation, Conceptualization. **Qiang Wang:** Software, Conceptualization. **Hong Li:** Visualization. **Haitao Zhou:** Data curation. **Wei Yi:** Writing – review & editing, Supervision. **Yang Sun:** Writing – review & editing, Supervision.

Study approval

All animal experimental protocols were approved by the Animal Care and Use Committee of the AFMU (approval number: NO.20241450).

Funding

This work was supported by the National Natural Science Foundation of China (grants no. 82270286), National Natural Science Foundation of China (grants no. 82170336), Xijing Hospital Innovative Medical Research Project – General project (XJZT24LY19) and Xijing Hospital Innovative Medical Research Project – General project (XJZT24CY35).

Declaration of competing interest

The authors declare that they have no known competing financial interests or personal relationships that could have appeared to influence the work reported in this paper.

Acknowledgements

The figures in this article, Figs. 1A–. 2A and 4A–. 6A, 7A and 9 were created using BioRender software (https://biorender.com).

Appendix A. Supplementary data

Supplementary data to this article can be found online at https://doi.org/10.1016/j.redox.2025.103580.

Data availability

Data will be made available on request.

References

[1] World Health Organization, The Global Burden of Disease: 2004 Update, WHO Press, Geneva, Switzerland, 2008.
[2] M.K. Jha, et al., Screening and Management of depression in patients with cardiovascular disease: JACC state-of-the-art review, J. Am. Coll. Cardiol. 73 (14) (2019) 1827–1845.
[3] D.L. Hare, et al., Depression and cardiovascular disease: a clinical review, Eur. Heart J. 35 (21) (2014) 1365–1372.
[4] C.A. Pivato, et al., Depression and ischemic heart disease, Int. J. Cardiol. 364 (2022) 9–15.
[5] S. Parashar, et al., Impact of depression on sex differences in outcome after myocardial infarction, Circ Cardiovasc Qual Outcomes 2 (1) (2009) 33–40.
[6] R. Meng, et al., Association of depression with all-cause and cardiovascular disease mortality among adults in China, JAMA Netw. Open 3 (2) (2020) e1921043.
[7] M.F. Piepoli, et al., European guidelines on cardiovascular disease prevention in clinical practice: the sixth joint task Force of the European society of Cardiology and other societies on cardiovascular disease prevention in clinical practice (constituted by representatives of 10 societies and by invited experts)Developed with the special contribution of the European association for cardiovascular prevention & rehabilitation (EACPR), Eur. Heart J. 37 (29) (2016) 2315–2381, 2016.
[8] J.S. Loh, et al., Microbiota-gut-brain axis and its therapeutic applications in neurodegenerative diseases, Signal Transduct Target Ther 9 (1) (2024) 37.
[9] E.A. Mayer, K. Nance, S. Chen, The gut-brain Axis, Annu. Rev. Med. 73 (2022) 439–453.
[10] M.D. Gershon, The Second Brain, HarperCollins, 1998.
[11] M.D. Gershon, K.G. Margolis, The gut, its microbiome, and the brain: connections and communications, J. Clin. Investig. 131 (18) (2021).
[12] C.A. Simpson, et al., The gut microbiota in anxiety and depression - a systematic review, Clin. Psychol. Rev. 83 (2021) 101943.
[13] P. Zheng, et al., Gut microbiome remodeling induces depressive-like behaviors through a pathway mediated by the host's metabolism, Mol Psychiatry 21 (6) (2016) 786–796.
[14] R.T. Liu, et al., Reductions in anti-inflammatory gut bacteria are associated with depression in a sample of young adults, Brain Behav. Immun. 88 (2020) 308–324.
[15] N. Kazemian, et al., Gut microbiota and cardiovascular disease: opportunities and challenges, Microbiome 8 (1) (2020) 36.
[16] W.H. Tang, S.L. Hazen, The gut microbiome and its role in cardiovascular diseases, Circulation 135 (11) (2017) 1008–1010.
[17] M. Witkowski, T.L. Weeks, S.L. Hazen, Gut microbiota and cardiovascular disease, Circ. Res. 127 (4) (2020) 553–570.
[18] A. Agus, J. Planchais, H. Sokol, Gut microbiota regulation of tryptophan metabolism in health and disease, Cell Host Microbe 23 (6) (2018) 716–724.
[19] H.M. Roager, T.R. Licht, Microbial tryptophan catabolites in health and disease, Nat. Commun. 9 (1) (2018) 3294.
[20] Y.C. Wang, et al., Indole-3-Propionic acid protects against heart failure with preserved ejection fraction, Circ. Res. 134 (4) (2024) 371–389.
[21] H. Xue, et al., Gut microbially produced indole-3-propionic acid inhibits atherosclerosis by promoting reverse cholesterol transport and its deficiency is causally related to atherosclerotic cardiovascular disease, Circ. Res. 131 (5) (2022) 404–420.
[22] E. Serger, et al., The gut metabolite indole-3 propionate promotes nerve regeneration and repair, Nature 607 (7919) (2022) 585–592.
[23] Y. Wang, et al., Multi-omics reveal microbial determinants impacting the treatment outcome of antidepressants in major depressive disorder, Microbiome 11 (1) (2023) 195.
[24] D.M. Bannerman, et al., Hippocampal synaptic plasticity, spatial memory and anxiety, Nat. Rev. Neurosci. 15 (3) (2014) 181–192.
[25] G. MacQueen, T. Frodl, The hippocampus in major depression: evidence for the convergence of the bench and bedside in psychiatric research? Mol Psychiatry 16 (3) (2011) 252–264.
[26] A. Wu, J. Zhang, Neuroinflammation, memory, and depression: new approaches to hippocampal neurogenesis, J. Neuroinflammation 20 (1) (2023) 283.
[27] X. Fang, et al., Ferroptosis as a target for protection against cardiomyopathy, Proc. Natl. Acad. Sci. U. S. A. 116 (7) (2019) 2672–2680.
[28] J. Lillo-Moya, et al., Targeting ferroptosis against ischemia/reperfusion cardiac injury, Antioxidants 10 (5) (2021).
[29] X. Chen, et al., Ferroptosis: machinery and regulation, Autophagy 17 (9) (2021) 2054–2081.
[30] A. Nègre-Salvayre, et al., Proatherogenic effects of 4-hydroxynonenal, Free Radic. Biol. Med. 111 (2017) 127–139.
[31] Y. Santin, et al., Mitochondrial 4-HNE derived from MAO-A promotes mitoCa(2+) overload in chronic postischemic cardiac remodeling, Cell Death Differ. 27 (6) (2020) 1907–1923.
[32] L. Liu, et al., Deubiquitinase OTUD5 as a novel protector against 4-HNE-triggered ferroptosis in myocardial ischemia/reperfusion injury, Adv. Sci. 10 (28) (2023) e2301852.
[33] W. Cai, et al., Alox15/15-HpETE aggravates myocardial ischemia-reperfusion injury by promoting cardiomyocyte ferroptosis, Circulation 147 (19) (2023) 1444–1460.
[34] L. Liu, et al., Gut microbiota and its metabolites in depression: from pathogenesis to treatment, EBioMedicine 90 (2023) 104527.
[35] W. Jia, G. Panagiotou, Recent advances in diabetes and microbiota, Sci Bull (Beijing) 67 (17) (2022) 1720–1723.
[36] W. Wei, et al., Psychological stress-induced microbial metabolite indole-3-acetate disrupts intestinal cell lineage commitment, Cell Metab. 36 (3) (2024) 466–483. e7.
[37] L. Cheng, et al., A Gpr35-tuned gut microbe-brain metabolic axis regulates depressive-like behavior, Cell Host Microbe 32 (2) (2024) 227–243.e6.
[38] Q. Li, et al., Associations between plasma tryptophan and indole-3-propionic acid levels and mortality in patients with coronary artery disease, Am. J. Clin. Nutr. 116 (4) (2022) 1070–1077.
[39] C. Xue, et al., Tryptophan metabolism in health and disease, Cell Metab. 35 (8) (2023) 1304–1326.
[40] S. Xu, et al., Naringenin alleviates myocardial ischemia/reperfusion injury by regulating the nuclear factor-erythroid factor 2-related factor 2 (Nrf2)/System xc-/glutathione peroxidase 4 (GPX4) axis to inhibit ferroptosis, Bioengineered 12 (2) (2021) 10924–10934.
[41] M. Zhang, et al., Activation of nrf2 by lithospermic acid ameliorates myocardial ischemia and reperfusion injury by promoting phosphorylation of AMP-activated protein kinase α (AMPKα), Front. Pharmacol. 12 (2021) 794982.
[42] J.F. Cryan, T.G. Dinan, Mind-altering microorganisms: the impact of the gut microbiota on brain and behaviour, Nat. Rev. Neurosci. 13 (10) (2012) 701–712.
[43] J.A. Foster, K.A. McVey Neufeld, Gut-brain axis: how the microbiome influences anxiety and depression, Trends Neurosci. 36 (5) (2013) 305–312.
[44] J.R. Kelly, et al., Transferring the blues: depression-associated gut microbiota induces neurobehavioural changes in the rat, J. Psychiatr. Res. 82 (2016) 109–118.
[45] D. Radjabzadeh, et al., Gut microbiome-wide association study of depressive symptoms, Nat. Commun. 13 (1) (2022) 7128.
[46] I. Łoniewski, et al., Major Depressive Disorder and gut microbiota - association not causation. A scoping review, Prog. Neuropsychopharmacol. Biol. Psychiatry 106 (2021) 110111.
[47] A. Kosuge, et al., Heat-sterilized Bifidobacterium breve prevents depression-like behavior and interleukin-1β expression in mice exposed to chronic social defeat stress, Brain Behav. Immun. 96 (2021) 200–211.
[48] F. Guida, et al., Antibiotic-induced microbiota perturbation causes gut endocannabinoidome changes, hippocampal neuroglial reorganization and depression in mice, Brain Behav. Immun. 67 (2018) 230–245.
[49] S. Nayfach, et al., New insights from uncultivated genomes of the global human gut microbiome, Nature 568 (7753) (2019) 505–510.
[50] S. Ahmadmehrabi, W.H.W. Tang, Gut microbiome and its role in cardiovascular diseases, Curr. Opin. Cardiol. 32 (6) (2017) 761–766.
[51] W. Hao, et al., Gut dysbiosis induces the development of depression-like behavior through abnormal synapse pruning in microglia-mediated by complement C3, Microbiome 12 (1) (2024) 34.
[52] Y. Liang, et al., Probiotic mixture of Lactobacillus and Bifidobacterium alleviates systemic adiposity and inflammation in non-alcoholic fatty liver disease rats through Gpr109a and the commensal metabolite butyrate, Inflammopharmacology 26 (4) (2018) 1051–1055.
[53] A. Kazemi, et al., Effect of probiotic and prebiotic vs placebo on psychological outcomes in patients with major depressive disorder: a randomized clinical trial, Clin Nutr 38 (2) (2019) 522–528.
[54] Y.S. Lee, et al., Microbiota-derived lactate accelerates intestinal stem-cell-mediated epithelial development, Cell Host Microbe 24 (6) (2018) 833–846.e6.
[55] W.H. Tang, T. Kitai, S.L. Hazen, Gut microbiota in cardiovascular health and disease, Circ. Res. 120 (7) (2017) 1183–1196.
[56] P. Zheng, et al., Plasma metabonomics as a novel diagnostic approach for major depressive disorder, J. Proteome Res. 11 (3) (2012) 1741–1748.
[57] P. Zheng, et al., A novel urinary metabolite signature for diagnosing major depressive disorder, J. Proteome Res. 12 (12) (2013) 5904–5911.
[58] P. Zheng, et al., Identification and validation of urinary metabolite biomarkers for major depressive disorder, Mol. Cell. Proteomics 12 (1) (2013) 207–214.
[59] M. Yu, et al., Variations in gut microbiota and fecal metabolic phenotype associated with depression by 16S rRNA gene sequencing and LC/MS-based metabolomics, J. Pharm. Biomed. Anal. 138 (2017) 231–239.
[60] W.T. Lai, et al., Shotgun metagenomics reveals both taxonomic and tryptophan pathway differences of gut microbiota in major depressive disorder patients, Psychol. Med. 51 (1) (2021) 90–101.
[61] Z. Wang, Y. Zhao, Gut microbiota derived metabolites in cardiovascular health and disease, Protein Cell 9 (5) (2018) 416–431.
[62] J.R. Liu, et al., Gut microbiota-derived tryptophan metabolism mediates renal fibrosis by aryl hydrocarbon receptor signaling activation, Cell. Mol. Life Sci. 78 (3) (2021) 909–922.
[63] W.R. Wikoff, et al., Metabolomics analysis reveals large effects of gut microflora on mammalian blood metabolites, Proc. Natl. Acad. Sci. U. S. A. 106 (10) (2009) 3698–3703.

[64] D. Dodd, et al., A gut bacterial pathway metabolizes aromatic amino acids into nine circulating metabolites, Nature 551 (7682) (2017) 648–652.
[65] M. Wlodarska, et al., Indoleacrylic acid produced by commensal Peptostreptococcus species suppresses inflammation, Cell Host Microbe 22 (1) (2017) 25–37.e6.
[66] W.Z. Hao, et al., A review of antibiotics, depression, and the gut microbiome, Psychiatry Res. 284 (2020) 112691.
[67] G. Wang, et al., Microbiota-derived indoles alleviate intestinal inflammation and modulate microbiome by microbial cross-feeding, Microbiome 12 (1) (2024) 59.
[68] Y. Hu, et al., Interplay between diet, circulating indolepropionate concentrations and cardiometabolic health in US populations, Gut 72 (12) (2023) 2260–2271.
[69] C.S. Kim, et al., Gut microbiota indole-3-propionic acid mediates neuroprotective effect of probiotic consumption in healthy elderly: a randomized, double-blind, placebo-controlled, multicenter trial and in vitro study, Clin Nutr 42 (6) (2023) 1025–1033.
[70] X. Fang, et al., The molecular and metabolic landscape of iron and ferroptosis in cardiovascular disease, Nat. Rev. Cardiol. 20 (1) (2023) 7–23.
[71] J. Zheng, M. Conrad, The metabolic underpinnings of ferroptosis, Cell Metab. 32 (6) (2020) 920–937.
[72] J. Yin, et al., Gut microbiota-derived indole derivatives alleviate neurodegeneration in aging through activating GPR30/AMPK/SIRT1 pathway, Mol. Nutr. Food Res. 67 (9) (2023) e2200739.
[73] T. Zelante, et al., Tryptophan catabolites from microbiota engage aryl hydrocarbon receptor and balance mucosal reactivity via interleukin-22, Immunity 39 (2) (2013) 372–385.
[74] Y. Cheng, et al., Aryl hydrocarbon receptor activity of tryptophan metabolites in young adult mouse colonocytes, Drug Metab. Dispos. 43 (10) (2015) 1536–1543.
[75] T.D. Hubbard, et al., Adaptation of the human aryl hydrocarbon receptor to sense microbiota-derived indoles, Sci. Rep. 5 (2015) 12689.
[76] B. Stockinger, et al., The aryl hydrocarbon receptor: multitasking in the immune system, Annu. Rev. Immunol. 32 (2014) 403–432.
[77] Z.B. Huang, et al., Gut microbiota-derived indole 3-propionic acid partially activates aryl hydrocarbon receptor to promote macrophage phagocytosis and attenuate septic injury, Front. Cell. Infect. Microbiol. 12 (2022) 1015386.
[78] H. Zhuang, et al., Indole-3-propionic acid alleviates chondrocytes inflammation and osteoarthritis via the AhR/NF-κB axis, Mol Med 29 (1) (2023) 17.
[79] C. Chen, et al., Microbial tryptophan metabolites ameliorate ovariectomy-induced bone loss by repairing intestinal AhR-mediated gut-bone signaling pathway, Adv. Sci. 11 (36) (2024) e2404545.
[80] Y. Zhang, et al., Pretreatment with indole-3-propionic acid attenuates lipopolysaccharide-induced cardiac dysfunction and inflammation through the AhR/NF-κB/NLRP3 pathway, J. Inflamm. Res. 17 (2024) 5293–5309.
[81] H. Chen, et al., Highly multiplexed bioactivity screening reveals human and microbiota metabolome-GPCRome interactions, Cell 186 (14) (2023) 3095–3110.e19.
[82] L.J. Cohen, et al., Commensal bacteria make GPCR ligands that mimic human signalling molecules, Nature 549 (7670) (2017) 48–53.
[83] L.M. Aleksunes, C.D. Klaassen, Coordinated regulation of hepatic phase I and II drug-metabolizing genes and transporters using AhR-, CAR-, PXR-, PPARα-, and Nrf2-null mice, Drug Metab. Dispos. 40 (7) (2012) 1366–1379.
[84] Y.D. Bhutia, et al., Gut microbiome and colon cancer: role of bacterial metabolites and their molecular targets in the host, Curr Colorectal Cancer Rep 13 (2) (2017) 111–118.
[85] M. Little, et al., Understanding the physiological functions of the host xenobiotic-sensing nuclear receptors PXR and CAR on the gut microbiome using genetically modified mice, Acta Pharm. Sin. B 12 (2) (2022) 801–820.
[86] T. Wang, et al., Microbiota-indole 3-propionic acid-brain axis mediates abnormal synaptic pruning of hippocampal microglia and susceptibility to ASD in IUGR offspring, Microbiome 11 (1) (2023) 245.
[87] J. Jiang, et al., The gut metabolite indole-3-propionic acid activates ERK1 to restore social function and hippocampal inhibitory synaptic transmission in a 16p11.2 microdeletion mouse model, Microbiome 12 (1) (2024) 66.
[88] X. Qian, et al., Bifidobacteria with indole-3-lactic acid-producing capacity exhibit psychobiotic potential via reducing neuroinflammation, Cell Rep Med 5 (11) (2024) 101798.
[89] S.Y. Shen, et al., The neuroprotective effects of GPR55 against hippocampal neuroinflammation and impaired adult neurogenesis in CSDS mice, Neurobiol. Dis. 169 (2022) 105743.
[90] X. Yu, et al., A specific circuit in the midbrain detects stress and induces restorative sleep, Science 377 (6601) (2022) 63–72.
[91] S.A. Golden, et al., A standardized protocol for repeated social defeat stress in mice, Nat. Protoc. 6 (8) (2011) 1183–1191.
[92] A.Q. Song, et al., NLRP1 inflammasome contributes to chronic stress-induced depressive-like behaviors in mice, J. Neuroinflammation 17 (1) (2020) 178.
[93] A. Armario, The forced swim test: historical, conceptual and methodological considerations and its relationship with individual behavioral traits, Neurosci. Biobehav. Rev. 128 (2021) 74–86.
[94] M.Y. Liu, et al., Sucrose preference test for measurement of stress-induced anhedonia in mice, Nat. Protoc. 13 (7) (2018) 1686–1698.
[95] G.W. Zhang, et al., Medial preoptic area antagonistically mediates stress-induced anxiety and parental behavior, Nat. Neurosci. 24 (4) (2021) 516–528.
[96] Q. Zhou, et al., Gut microbiome mediates the protective effects of exercise after myocardial infarction, Microbiome 10 (1) (2022) 82.
[97] V. Stratoulias, et al., ARG1-expressing microglia show a distinct molecular signature and modulate postnatal development and function of the mouse brain, Nat. Neurosci. 26 (6) (2023) 1008–1020.
[98] H. Zhuang, et al., Long-term high-fat diet consumption by mice throughout adulthood induces neurobehavioral alterations and hippocampal neuronal remodeling accompanied by augmented microglial lipid accumulation, Brain Behav. Immun. 100 (2022) 155–171.
[99] S. Silvestro, et al., MicroRNA profiling of HL-1 cardiac cells-derived extracellular vesicles, Cells 10 (2) (2021).
[100] W. Zhu, et al., Macrophage migration inhibitory factor facilitates the therapeutic efficacy of mesenchymal stem cells derived exosomes in acute myocardial infarction through upregulating miR-133a-3p, J Nanobiotechnology 19 (1) (2021) 61.